Practical Medical Applications of Quantitative MR Relaxometry

Hai-Ling Margaret Cheng, Nikola Stikov, Nilesh R. Ghugre, Graham A. Wright

Practical Medical Applications of Quantitative MR Relaxometry

Journal:	*Journal of Magnetic Resonance Imaging*
Manuscript ID:	JMRI-11-0882.R1
Wiley - Manuscript type:	Invited Review
Classification:	Relaxation theory and measurement < Imaging technology and safety < Basic Science, Imaging techniques and processing < Imaging technology and safety < Basic Science, Education < Imaging Principles and Education < Basic Science
Manuscript Keywords:	T1 relaxation, T2 relaxation, T2* relaxation, multiple sclerosis, iron overload, myocardial infarction

Practical Medical Applications of Quantitative MR Relaxometry

Hai-Ling Margaret Cheng, PhD[1,2], Nikola Stikov, PhD[3], Nilesh R. Ghugre, PhD[4], *Graham A. Wright, PhD [2,4,5]

[1] *Physiology & Experimental Medicine, Research Institute, The Hospital for Sick Children, Toronto, ON, Canada*
[2] *Department of Medical Biophysics, University of Toronto, Toronto, ON, Canada*
[3] *McConnell Brain Imaging Centre, Montreal Neurological Institute, McGill University, Montreal, QC, Canada*
[4] *Imaging Research, Sunnybrook Research Institute, Toronto, ON, Canada*
[5] *Schulich Heart Program, Sunnybrook Health Sciences Centre, Toronto, ON, Canada*

*Corresponding Author:

Graham A. Wright
Senior Scientist
Imaging Research
Sunnybrook Research Institute
2075 Bayview Ave., Rm. S656
Toronto, ON
Canada, M4N 3M5

Tel: (416) 480-6869
Fax: (416) 480-5714

Email: gawright@sri.utoronto.ca

Running Title: Applications of MR Relaxometry

Practical Medical Applications of Quantitative MR Relaxometry

ABSTRACT

Conventional magnetic resonance (MR) images are qualitative, and their signal intensity is dependent on several complementary contrast mechanisms that are manipulated by the MR hardware and software. In the absence of a quantitative metric for absolute interpretation of pixel signal intensities, one that is independent of scanner hardware and sequences, it is difficult to perform comparisons of MR images across subjects or longitudinally in the same subject. Quantitative relaxometry isolates the contributions of individual MR contrast mechanisms (T1, T2, T2*) and provides maps, which are independent of the MR protocol and have a physical interpretation often expressed in absolute units. In addition to providing an unbiased metric for comparing MR scans, quantitative relaxometry utilizes the relationship between MR maps and physiology to provide a non-invasive surrogate for biopsy and histology. This paper provides an overview of some promising clinical applications of quantitative relaxometry, followed by a description of the methods and challenges of acquiring accurate and precise quantitative MR maps. It concludes with three case studies of quantitative relaxometry applied to studying multiple sclerosis, liver iron, and acute myocardial infarction.

Keywords: T1 relaxation, T2 relaxation, T2* relaxation, multiple sclerosis, iron overload, myocardial infarction

INTRODUCTION

Conventional magnetic resonance (MR) images provide excellent tissue contrast, but the signal intensity at any pixel can only be interpreted qualitatively. It is difficult to assign meaning in terms of underlying biophysical or physiological properties on the basis on image signal intensity alone. The reason is that the MR signal is influenced by a number of intrinsic contrast mechanisms, such as the density of water protons and proton relaxation times (T1, T2, T2*). These are emphasized to different degrees depending on the image acquisition sequence chosen. Interpreting MR images, therefore, requires selection of an appropriate sequence and a thorough understanding of the corresponding signal contrast in relation to underlying pathophysiology. That said, signal intensity also depends on characteristics of the imaging system such as coil sensitivities. Therefore, evaluation remains qualitative and subjective, and comparisons across different scanner hardware and acquisition sequences are difficult, typically being restricted to descriptions of relative contrast between different anatomical regions. In order to obtain information on tissue structure and function in a quantitative manner, independent of scanner hardware and sequence parameters, we need to extract the contributions of different contrast mechanisms from the MR signal. Only with such decomposition may one consider using MRI as a measuring device to probe tissue properties on an absolute and quantitative level.

Quantitative MRI refers to the measurement of biophysical parameters through decoupling the different contrast mechanisms that contribute to the overall MR signal. Some of the fundamental quantitative MRI parameters reflecting the local tissue environment are the relaxation times T1, T2, and T2*. Quantitative measurement of relaxation parameters has a long and illustrious history in the study of nuclear magnetic resonance going back to the first paper on the subject by Bloembergen et al. (1). In 1986, Koenig and colleagues introduced the term “relaxometry” for the measurement of T1 as a function of magnet field strength (2). The term has since been adopted by the MRI community to refer to relaxation measurement in general. Recognizing the convenience of compact nomenclature, we follow this convention and henceforth refer to the measurement of relaxation times in MRI as relaxometry and images representing the spatial distribution of relaxation times as T1, T2, or T2* maps.

The advantages of quantitative imaging are varied. One obvious advantage is the removal of influences unrelated to tissue properties, such as those involving operator dependency, differences in scan parameters, spatial variation in the magnetic field, and image scaling. Quantitation, therefore, allows comparisons across different sites and MRI protocols, and enables large-scale multi-institutional studies on patient cohorts. Not only can comparisons be made

between different patients, but measurements can be followed longitudinally within the same patient, for example, to follow the course of treatment. Problems of bias and reproducibility are greatly reduced, allowing biological changes with disease progression and response to therapy to be probed in a more satisfactory manner. Ultimately, the value of quantitation is fully reaped when MRI can provide "measurements" of biological properties in a way similar to current gold-standard techniques such as biopsy and histology. By providing quantitative physiologically-relevant information in a non-invasive manner and throughout a three-dimensional (3D) volume at high spatial resolution, quantitative MRI can potentially serve as the ideal surrogate, unfettered by conventional limitations of limited biopsy sampling or the possibility of sampling error.

What follows is an overview of the clinical applications of quantitative relaxometry, followed by a description of the methods and challenges of acquiring accurate and precise quantitative MRI maps. We limit the scope of this review to T1, T2 and T2* mapping, as these are the fundamental MR quantities that form the basis of quantitative relaxometry.

CLINICAL MOTIVATION

Quantitative relaxometry has been used extensively in research studies of pathophysiology in the brain, body and heart. Here, we briefly survey work in these areas where we believe quantitative MRI could have a significant impact on clinical management.

Brain

Brain pathology is often associated with prolongation of the T1, T2 and T2* relaxation times. There has been a number of papers reporting a global increase in the brain relaxation times in conditions as varied as autism (3), dementia (4), and Parkinson's disease (5). The relaxation time increase presents as hyperintensity on T2-weighted images and hypointensity on T1-weighted scans, but quantifying the T1 and T2 parameter has been shown to increase pathological specificity and to help differentiate between healthy and affected tissue locally within a subject. Relaxometry also shows great promise for quantifying iron content in the brain and understanding its role in disease (6). In this review we focus on multiple sclerosis, brain tumors, stroke, and epilepsy - the four clinical conditions that have seen the greatest exposure to relaxometry studies. For a more comprehensive review of brain relaxometry applications, please refer to (7).

Multiple Sclerosis

T2-weighted scans are commonly used to diagnose multiple sclerosis, due to their sensitivity to altered tissue water content in MS lesions. However, T2-weighted scans lack pathological specificity. In particular, it is difficult to differentiate between inflammation, edema, gliosis, demyelination and axonal loss, and the relationship between T2 lesion load and the disability measure is poor (8,9).

While classically regarded as a white matter disease, multiple sclerosis is characterized by changes in the relaxation times in both grey and white matter. There have been reported whole-brain T1 histogram shifts, which are more pronounced in secondary progressive MS (10), but are also present in the primary progressive (11) and relapsing-remitting stages of the disease (12). The histogram peak positions are correlated with clinical disability (10,11), but not with the T2 lesion load (10,12).

T1 contrast also contributes to increasing the local pathological specificity, particularly in studying T1-hypointense lesions called 'black holes', as well as in studying grey matter pathology. T1 hypointensity has been correlated with axonal loss (13), and a correlation between T1 lesion load and disability has been demonstrated using histopathology (14), and MR spectroscopy (15). A recent paper that compared relaxometry against immunohistochemistry in fixed tissue also showed increases in the relaxation times in grey matter cortical lesions compared to normal appearing grey matter (16). A T1 analysis in the hypothalamus shows the same trend, with significant fatigue severity correlation (17).

A quantitative T2 measure called myelin water fraction (MWF) is a useful MS biomarker that increases the pathological specificity to myelin loss (18). The myelin water fraction is computed from a multi-exponential T2 fit, where the short T2 component (T2~10-50ms) is assigned to water trapped between the myelin sheaths. The myelin water fraction correlation with myelin loss has been validated with histopathology (19). Recently, T2* mapping has shown great promise in characterizing the role of veins and iron in MS (6,20).

For a more in-depth look at relaxometry in multiple sclerosis, the reader can refer to (20,21).

Tumors

While tumors are studied routinely using qualitative MRI, quantification has the potential to eliminate the need for invasive procedures to determine tumor types. It is well-established that T1 values within tumors are longer than normal white matter values (22,23), but there are also differences in the T1 values across tumor types. For example, meningiomas and pituitary tumors

have the shortest T1 values, which are still longer than in normal tissue. Glioblastomas on the other hand, have the longest T1 values (24).

The fast uptake of contrast agents due to the breakdown of the blood-brain barrier (BBB) is the foundation of dynamic contrast-enhanced MRI (DCE-MRI) (25,26). T1 and T2* relaxometry as part of the DCE-MRI protocol has been used for detection of primary and metastatic tumors, inflammation, demyelination and ischemia (27), as well as for noninvasive grading of brain gliomas (28). DCE-MRI has also shown that there is a high correlation between microvascular permeability and tumor grade (29).

Stroke

In stroke, ischemic areas and infarctions are characterized by T1 and T2 prolongation (30). While diffusion imaging remains the standard for determining extent of damage, relaxometry maps can help differentiate between salvagable and non-salvagable tissue (3). While T1 mapping can be used for detecting haemorrhagic change within infarcts (30), acquiring a T2 map is useful for improving specificity in distinguishing infarction from ischemic penumbra (31). Lansberg et al. showed that T2 mapping helped differentiate new lesions from lesions older than 36 hours, a task which is difficult to do visually (32). DCE-MRI has also been used for evaluating stroke extent and severity by generating cerebral blood flow (CBF) maps comparable to those obtained from PET studies (33).

Epilepsy

Relaxometry maps reveal increased T1 and T2 values in the temporal lobe, particularly in the hemisphere containing the seizure focus (34-36). Quantitative measurement of hippocampal T2 relaxation time (HCT2) provides additional sensitivity in identifying brain abnormalities in temporal lobe epilepsy (37,38), especially in epilepsy patients with normal hippocampal volume (39).

Body

Applications of quantitative relaxometry in the body are varied and remain to be fully explored. To date, the value of quantitation is established for the evaluation of iron overload and cartilage disease. Assessment of tumors, diffuse liver disease, and disorders of the kidney, spleen, and pancreas has also benefited from quantitative relaxometry.

Iron Overload

One of the few widely used clinical applications of quantitative relaxometry is measurement of iron overload in the body (40). Iron is used in the production of hemoglobin and is usually stored in the liver and spleen. In several pathologies, accumulation of iron occurs as a result of frequent blood transfusions to treat anemia (e.g. thalassemia, sickle cell disease) or as a result of excess iron absorption (e.g. hereditary hemochromatosis). Without treatment, excess iron can kill after injuring different body organs, and the goal of treatment is to prevent liver damage and heart failure. Relaxation times (T1, T2, T2*) shorten in the presence of iron compared to those in normal tissue. Quantitative T2 and T2* relaxometry has proven to be an accurate non-invasive means to measure absolute iron content and has replaced gold-standard biopsy procedures in many centers. In the liver, where iron first accumulates in the body, absolute iron levels have been calibrated against both T2 (41) and T2* (42). MRI quantification has also been performed to evaluate iron loading in extra-hepatic organs such as the pancreas, spleen (43,44) and kidney (45). A more recent focus is the utility of MRI iron quantification for evaluating and comparing different chelation therapy regimes aimed at reducing iron burden (46).

Cartilage Disease

Osteoarthritis, rheumatoid arthritis, and other degenerative conditions of the cartilage have benefited greatly from quantitative relaxometry to detect early chondral degeneration and biochemical changes before gross morphological alterations occur (47). Early detection is key to intervention when damage is still potentially reversible (48,49). A variety of quantitative MRI parameters, including T1, T2, and T2*, have been used to measure different biophysical and biochemical aspects of cartilage disease. For example, proteoglycan depletion can be quantified with T1 following the injection of a gadolinium-based contrast agent (50). Changes in collagen content can be quantified using T2* and T2, with T2 providing additional information on collagen organization (51,52). Multicomponent T2 analysis can give more specific insight into changes in collagen content (53). Even T1 has recently been shown to be moderately correlated with collagen (54). In addition to providing early diagnosis, quantitative relaxometry has also been used to follow cartilage repair treatment, such as microfracture, autologous cartilage transplantation, or osteochondral transplantation (55).

Injury and Infection

Although MRI relaxometry is not widely used in the clinic for assessment of injury and infection, a number of studies have indicated its potential for more specific diagnosis. In diffuse

liver disease, especially in fatty liver disease, T1 relaxation times vary depending on acuteness of injury, so that acute forms of fatty liver disease prolong T1 while chronic forms of injury tend to shorten T1 (56). In the kidney, T1 has shown potential as a reliable marker of injury, including edema, inflammation, and fibrosis (57). In muscle, where inflammation can arise from injury or infection (58), T1 and T2 relaxation times can improve diagnostic specificity over conventional MRI of edema and inflammation. For example, T2 has been correlated to the degree of muscle weakness and muscle enzyme levels (59), and T1 changes can be used to map the distribution of contrast agent for early identification of inflammation and response to therapy (60).

Cancer

Quantitative relaxometry is normally applied to determine vascular patterns and malignant potential of tumors. This is performed through a dynamic contrast-enhanced (DCE) protocol, where T1 quantification is necessary to estimate the perfusion and endothelial permeability of tumor blood vessels. DCE-MRI has demonstrated the best potential of all quantitative MRI methods for tumor characterization, staging, and therapy monitoring (61). However, quantitative relaxometry has value even outside of the DCE-MRI exam. Improved distinction of malignant lesions from normal or benign tissue has been suggested, as in using T1 and T2 to differentiate colorectal metastases from normal liver (62) or malignant and benign liver lesions (63). Tumor therapy can also benefit from quantitation in a variety of ways. For example, thermal ablation can be guided using T1-based MR thermometry for measuring temperature in real-time (64). Tumour hypoxia can be quantified using T2*, as demonstrated in experimental strategies to improve (65) or decrease (66) tumor oxygenation. Post-therapy tissue changes are also better distinguished. In this role, DCE-MRI is the traditional approach, used to distinguish residual tumor from vascular granulation tissue (67). However, T1 and T2 changes without contrast agent are also useful, as in assessing radiation therapy in soft tissue sarcoma (68). Proton density has demonstrated even greater accuracy than T1 or T2 in the case of imaging treated liver metastases (69) or liver radiofrequency-induced ablation (70).

Cardiac

The soft tissue contrast offered by intrinsic MRI relaxation mechanisms has been well exploited to demonstrate differences between normal and pathological conditions in the heart muscle. In addition, quantitative relaxometry can help grade severity of disease and monitor treatment progress in several cardiomyopathies.

Iron Overload

The utility of quantitative relaxometry has perhaps been best demonstrated in the management of patients suffering from cardiac iron overload (like thalassemia, sickle cell and hereditary hemochromatosis). A seminal paper by Anderson et al. described the relationship between myocardial T2* and left ventricular ejection fraction in patients with thalassemia major (71). It was found that patients with myocardial T2*<20 ms exhibited a proportional decline in ejection fraction indicative of an association between iron concentration and cardiac dysfunction. Unlike liver, where both T2 and T2* parameters have been calibrated for tissue iron concentration via clinically ordered biopsy (41,42), *in vivo* validation for cardiac iron stores is challenging due to the risk involved with cardiac biopsy. However, recent human autopsy studies (72,73) and preclinical studies (42) have suggested that similar relaxivity-iron calibrations can be derived for cardiac tissue as well. Recent preclinical studies have also demonstrated how relaxation measurements can help predict the clearance of iron based on type of iron chelator and acuity of iron loading in the heart (74,75).

Myocardial Infarction

In the case of acute myocardial infarction (AMI) or heart attack, early restoration of coronary blood flow is critical in order to limit cellular necrosis, maintain normal heart function and reduce adverse left ventricular (LV) remodeling and thereby prevent heart failure (76). Despite successful reperfusion, the *in vivo* pathophysiological processes (necrosis, inflammation, hemorrhage, fibrosis) occurring post-AMI have complicated interactions that are not well understood. MRI relaxation times T1, T2 and T2* are accordingly altered based on the state of the tissue damage – acute, sub-acute or chronic (77).

o *Edema/Inflammation* – The inflammatory state is typically reflected by the presence of edema. T2-weighted signal has been found to increase under edematous conditions due to short molecular correlation times in free water. Exploiting this effect, T2-weighted imaging has been popular in the clinic (78) however it is disadvantaged by issues with coil sensitivity correction and the inability to monitor serial progress. Alternatively, several groups are slowly pushing towards quantitative T2 mapping (79,80). Quantitative T2 allows monitoring the inflammatory state regionally and serially as well as across subjects – this will be most instrumental when interrogating novel anti-inflammatory strategies.

o *Hemorrhage* – The occurrence of intramyocardial hemorrhage as part of the reperfusion injury in AMI has been well documented in both humans (81) and animal models of myocardial infarction (82). Hemorrhagic infarcts have also been shown to produce the worst clinical outcomes. Similar to the application of iron overload, relaxation times are modulated in the presence of hemorrhage, although in a more complicated manner depending on the form of the heme iron (77). In general, T2 shortening has been used to identify hemorrhage (83), however, T2* is more sensitive and specific to iron degradation products of hemorrhage (80). Unlike brain hematoma/hemorrhage, the pathophysiology and evolution of myocardial hemorrhage in the setting of AMI along with its clinical impact is currently not well understood.

o *Methemoglobin* – Methemoglobin has been shown to demonstrate paramagnetic T1 shortening in brain hemorrhage. The effect has been attributed to structure of the protein that allows nearby water molecules to access the heme iron core (77). Presence of methemoglobin has been found to be associated with oxidative stress, resulting in lipid oxidation (84). Quantitative T1 has been utilized to assess methemoglobin formation after myocardial infarction (85) and may potentially be useful to probe effects of novel therapies on disease progression.

o *Vasodilator Function*: Coronary vasodilator dysfunction has been demonstrated in infarcted as well as remote myocardium in patients with acute coronary syndrome (86). Blood-oxygen-level-dependent (BOLD) imaging with T2* and T2 offers a novel way to probe myocardial perfusion reserve and oxygenation state by exploiting the paramagnetic properties of deoxyhemoglobin in blood (87,88). It has recently been demonstrated that T2-based BOLD effects can identify impaired vasodilator function in infarcted and remote myocardium after AMI (89).

o *Infarct and Grayzone* – Infarct characterization in ischemic cardiomyopathy is routinely performed using delayed hyperenhancement (DHE) of myocardium following contrast agent injection by acquiring inversion-recovery-based T1-weighted images. The DHE images can also provide information on infarct grayzone (mixture of viable and nonviable myocytes), which has been correlated with mortality (90) and inducibility for ventricular tachycardia (91). Since infarct and grayzone sizes are determined from single images, the calculations are prone to errors/variability arising from manual contouring of blood, image noise and subjectively chosen remote (uninfarcted) myocardium. It has been demonstrated that T1 quantification may be advantageous in this scenario offering greater reproducibility and reduced noise sensitivity (92,93).

Other Potential Applications

T1 and T2 relaxation times have been shown to reduce in chronic infarcts compared to remote myocardium as studied in human autopsy specimens (94); this behavior has been attributed to collagen deposition. Quantitative T1 has been utilized to estimate myocardial blood volume and myocardial perfusion using an intravascular contrast agent, allowing estimation of myocardial perfusion reserve (95). Elevated T2 may potentially be useful to assess acute inflammatory response in non-ischemic cardiomyopathies such as acute myocarditis where edema is of diffuse pattern rather than focal, hypertrophic cardiomyopathy and sarcoidosis (96,97). In heart transplants T2 elevation has also been associated with transplant rejection (98). Myocardial fibrosis is the hallmark of the failing heart and has been associated with systolic dysfunction, abnormal remodeling and increased ventricular stiffness (99). More recently, pre- and post-contrast T1 mapping has shown promise for detecting diffuse patterns of myocardial scarring/fibrosis in various non-ischemic cardiac pathologies such as diabetic, hypertensive, dilated and hypertrophic cardiomyopathy as well as in heart transplant cases (100). Quantitative relaxometry has offered a novel path to reveal interesting patterns in many such clinical applications, however most are currently only in the research phase and translation to the clinic is pending due to technical challenges.

Summary

As illustrated in the clinical examples described, quantitative relaxometry enables a more specific diagnosis of a wide range of diseases. This is due to the relationship between relaxation parameters and several fundamental pathophysiological properties that are common to many conditions. The relaxation time T1 is sensitive to macromolecular content, water content, and dissolved oxygen. Therefore, it has proven value in evaluating the loss of myelin and axons in brain, loss of proteoglycan in cartilage, collagen and methemoglobin content in the heart, and edema in the brain and heart. When an exogenous T1-reducing contrast agent such as Gd-DTPA is injected intravenously, analyzing the T1 reduction and its distribution in tissue enables assessment of tumor vessel blood flow and leakiness, breakdown of the blood-brain-barrier, infarct and grayzone regions in the heart, and fibrosis.

The relaxation time T2 is sensitive to tissue composition and structure, water content, and iron levels. It has been used to assess myelin content in the brain, collagen content and organization in cartilage and heart muscle, edema (i.e. inflammation), hemorrhage, and iron

content in the liver and heart. The relaxation time T2* is sensitive to deoxyhemoglobin, water content, and has even better sensitivity than T2 to iron levels. It has been used to assess brain function (due to altered deoxyhemoglobin levels), myocardial oxygenation, tumor hypoxia, hemorrhage, calcification in the heart (low water content), and liver and cardiac iron. The following section describes the physical mechanisms underlying T1, T2, and T2* to provide a better understanding of their relationship to pathophysiological properties.

PHYSICS OF RELAXOMETRY

Physical Principles and Biological Basis

The relaxation times T1, T2, and T2* are physical parameters determined by intrinsic biophysical properties of tissue. The longitudinal relaxation time, T1, is a time constant describing the recovery of magnetization from a perturbed state to its equilibrium state. This recovery is influenced by the fluctuating magnetic fields at the proton resonance frequency caused from neighboring atoms. Due to its proximity, the dominant source of fluctuations is typically the adjacent proton on the water molecule; the random tumbling of the water molecule, described by a rotational correlation time alters the angle between the protons over time and is the source of the magnetic fluctuation. When the rotational correlation time is equal to the inverse of the proton resonance frequency, T1 relaxation due to this interaction is fastest. Similarly, protons in lipids, particularly triglycerides, are affected by adjacent protons. Since protons in lipids are less mobile, there tends to be more energy at the proton resonance frequency, resulting in shorter T1s for lipds. Therefore, T1 provides an indication of the mobility of molecules (mainly water protons) and their binding to macromolecules. It is used primarily to assess macromolecular content, water binding, and water content in a variety of pathologies, including altered myelin content in the brain and inflammation. Beyond intrinsic tissue effects on T1, T1 can be altered through the introduction of a paramagnetic material, such Gd-DTPA, an intravenously administered contrast agent. The gadolinium in this agent forms a strong paramagnetic center, disrupting the local magnetic field. Water molecules tumbling and diffusing past this molecule experience substantial magnetic fluctuations; in particular, fluctuations at the resonance frequency of the water protons drive more rapid T1 relaxation. This application is particularly useful for quantifying properties of blood vessels, such as perfusion and blood volume.

The transverse relaxation time, T2, is a time constant describing the decay of magnetization that has been “excited” by a radio-frequency (RF) pulse (i.e. tipped into the

transverse plane) that cannot be reversed by refocusing pulses. This effect is due to random fluctuations in time of proton spins' resonant frequencies. Because spins precessing at different frequencies no longer accumulate phase at exactly the same rate, phase coherence is lost (i.e. dephasing) and the transverse magnetization decays. In biological tissue, a relatively rapid dephasing effect is seen in solids due to the presence of relatively slow fluctuations, which cause a large net phase dispersion. Protons bound to slowly tumbling macromolecules similarly experience rapid T2 decay, while relatively mobile protons (e.g. in water) decay much more slowly since rapid fluctuations tend to average out yielding a smaller net phase dispersion over time. In general, the random magnetic field fluctuations driving T2 decay are much slower (on the order of a few cycles/sec) than those driving T1 decay (where the driving fluctuations are on the order of tens of millions of cycles/sec corresponding to the resonance frequency).

The effective transverse relaxation time in the absence of refocusing pulses, T2*, is essentially T2 plus an additional relaxation term describing additional dephasing associated with variations in proton resonance frequencies within a volume that are constant over time; these variations cause dephasing within the volume over a period τ which can be unwound by suddenly changing the phase of all spins by 180 degrees using refocusing pulses and then letting phase evolve for another period τ. This reversible dephasing acts on top of the irreversible dephasing generated by random thermally driven molecular tumbling which causes T2 decay in the sample to create a net decay with the shorter time constant T2* in the absence of refocusing pulses. Any inhomogeneity in the local static field, such as those arising from imperfections in the magnet or from susceptibility differences at air-tissue interfaces or from the presence of paramagnetic or ferromagnetic substances, will result in such additional reversible dephasing. For these reasons, T2* is particularly useful for assessing body iron levels, deoxyhemoglobin content (blood oxygen), and imaging applications involving the use of iron oxide contrast agents – iron particles are substantial sources of local static magnetic field inhomogeneities.

Acquisition Sequences for Measuring Relaxation Times

Measurement of relaxation times is much more involved than acquiring a single image that depicts signal contrast amongst different tissue types. Typically, a series of images are acquired, each weighted slightly differently, to sample the recovery or decay of MR signal. A large number of images is generally required in this series to ensure adequate sampling of signal evolution and, therefore, accurate measurement of relaxation times. As a result, acquisition times

tend to be long. The following sections describe the basic relaxometry sequences and different variants tailored to specific clinical challenges.

T1 mapping

The gold standard for T1 mapping is known as inversion recovery (IR) (Fig. 1a) and consists of inverting the longitudinal magnetization Mz and sampling the MR signal as it recovers according to the Bloch Equation:

$$\frac{d}{dt}Mz(t) = \frac{\left[M_0 - Mz(t)\right]}{T1} \quad [1]$$

The IR sequence consists of two RF pulses, separated by an inversion time TI (Fig. 2). This sequence is repeated N times for each phase encode, varying the TI to produce N samples along the T1 recovery curve. The first RF pulse inverts the magnetization Mz, which then recovers with relaxation time T1. The second pulse tips the recovered longitudinal magnetization into the transverse plane. A variation of this approach is a saturation recovery sequence, where instead of inversion, the first pulse is a saturation pulse that tips the magnetization into the transverse plane and there is no second pulse. For either approach, the sequence is repeated a number of times, each time with a unique TI or TR as appropriate, to sample to recovery curve. The recovery curve is then fitted to an exponential model, which is an accurate representation only when several assumptions are met, including a perfect inversion pulse, constant temperature, or TR>>T1. While these assumptions are often justified, care must be taken to always pick a model that corresponds to the acquisition scheme (101).

While inversion recovery and saturation recovery offer accurate and precise T1 measurements, both techniques are too slow to be used in clinical practice because they require long TRs and acquire only one phase encode per TR. To speed up the acquisition, several variants have been proposed, such as following the inversion pulse by a fast spin-echo (FSE) (102) or echo-planar imaging (EPI) readout (103).

The Look-Locker (LL) method (104) is a rapid technique that measures T1 from a single recovery of longitudinal magnetization. It overcomes the limitation of the conventional IR method of requiring a long delay (on the order of T1) for longitudinal magnetization to recover until the next inversion pulse is played for subsequent readout. This novel approach was first theorized by Look and Locker and later implemented on a whole-body scanner by Brix et al. in the form of TOMROP (*T* *O*ne by *M*ultiple *R*ead*O*ut *P*ulses) (15). The basic sequence diagram is shown in Fig. 1b. It consists of only a single inversion pulse followed by a series of very small angle excitation (α) pulses with gradient echo readouts to sample the T1 curve. Since small angle

RF pulses are used, the longitudinal magnetization is only minimally disrupted during T1 recovery and no wait-period is necessary until equilibrium is reached as sampling is performed in a continuous manner. However, if the separation between α pulses is less than T2, the T1 signal will be corrupted by residual transverse magnetization gathered from previous α pulses. To avoid this, either the separation between the α pulses needs to be >5×T2 or gradient spoiling needs to be employed to crush any residual transverse magnetization. It is also important to note that due to continuous perturbation of the magnetization by successive α pulses, the recovery is driven into equilibrium more quickly, resulting in an '*effective T1'* or *T1** given by,

$$T1^* = \frac{T1}{\left[1 - \frac{T1}{TR^{\ln(\cos\alpha)}}\right]} \qquad [2]$$

The T1* calculated from the recovery curve needs to be converted to the *'actual'* T1 using the above equation. Recently, several other variants of the LL method have been developed targeted for specialized applications. For example, in the case of cardiac T1 mapping, basic LL cannot be applied due to severe cardiac and respiratory motion. A *MO*dified *LL* *I*nversion recovery sequence (MOLLI) has been proposed by Messroghli et al. for high resolution T1 mapping of the heart (105). Another variant using saturation recovery (MLLSR) instead of inversion recovery is also being investigated (106).

A different approach to rapid T1 measurement is to vary the flip angle of a gradient recalled sequence (107) (Fig. 1c). This method offers volumetric, high spatial resolution 3D T1 mapping in significantly less time than conventional methods. The time gain stems from the use of a short TR, unlike the conventional approach where TRs must be long to allow full signal recovery. The main source of error, however, is imperfect tipping of magnetization due to an inhomogeneous RF field. This error can be corrected efficiently by incorporating rapid B1 measurement of the RF field, which maintains a short acquisition time but significantly improves measured T1 accuracy (108). The practicality of this method for large volumetric T1 mapping has been recently demonstrated in various quantitative body protocols (109-111).

T2 mapping

The gold standard for T2 mapping is a Carr-Purcell-Meiboom-Gill (CPMG) spin-echo sequence (Fig. 3). It involves taking measurements at different echo times (i.e. TE= 2τ) in an echo train to sample the T2 decay curve. A 90 degree excitation pulse is followed by a series of 180 degree refocusing pulses, and signal is measured at the mid-points between refocusing pulses where the spin-echo is formed and B0 inhomogeneities are removed. While the number of echoes

is arbitrary, for a single-exponential fit (S = S0 exp(-TE/T2)) it is necessary to acquire at least two echoes. More echoes increase the accuracy and precision of single component T2 mapping, with long echo train lengths (32 and above) reserved for multicomponent T2 analysis (112).

A simpler implementation of the above method is to acquire a series of T2-weighted spin-echo datasets, each at a different TE. However, due to the long TR required, the acquisition time becomes prohibitively long for clinical practice. A much faster method was recently proposed by Sussman et al. (113). This method retains a conventional single-echo spin-echo acquisition but uses a constant difference of TR-TE (rather than a fixed long TR value) to reduce acquisition time by a factor of at least 4 to 6. Another rapid T2 mapping approach is to use a fast SSFP acquisition, which uses a fundamentally different contrast that is derived from a gradient-echo formation (114).

Magnetization prepared T2 measurement is another technique for efficient T2 mapping, particularly in the presence of blood flow and motion. In a conventional T2 spin echo sequence, signal contrast is primarily determined by placing the data acquisition block at the appropriate time (TE) following magnetization tip down by the RF pulse (Fig. 4a). An alternative strategy is to prepare the longitudinal magnetization in advance such that it represents the desired T2-weighted contrast and then sample it using any readout strategy (Fig. 4b) (115). This approach is very efficient and especially useful for obtaining T2 measurements in organs, such as the heart, where flow and motion produce undesirable artifacts. If a fast spin echo (FSE) approach is used, the readout is limited by tissue T2 relaxation time, which is generally short (~50 ms for the heart). On the other hand, the magnetization prepared signal is maintained on the order of time scale T1 (~1000 ms for the heart). In cases where relaxation properties of blood are to be interrogated, FSE may be highly susceptible to flow artifacts and hence other readout strategies (like GRE or SSFP) may be preferable in conjunction with T2-prepared contrast. Figure 4c shows an example of a sequence utilizing T2-prepared contrast. In the preparation block, the magnetization is first tipped down by a 90 RF pulse and then refocused by a specified number of 180 pulses to obtain a desired TE. Then the T2-weighted magnetization is tipped back up onto the longitudinal axis for subsequent readout. In this case, a spectro-spatial RF pulse has been shown (for fat suppression) with a spiral data acquisition strategy. The T2-prepared spiral readout sequence has been recently adopted to measure myocardial edema by T2 quantification following acute myocardial infarction in both clinical and preclinical models (80,116). Recently a T2-prepared SSFP sequence has also been developed for edema detection in myocardial infarction (79).

T2* mapping

T2* measurements are typically performed using a spoiled gradient echo sequence with multiple echoes (i.e. multi-echo gradient-echo) as illustrated in Fig. 5. Following a 90 degree RF excitation, signal is sampled at gradient echo formation generated by applying a series of alternating readout gradients; the phase encoding blip gradient determines the readout location in k-space. Typically, eight echoes are acquired within a TR interval and each echo corresponds to a different T2*-weighted image as determined by TE. Imaging is complete when the entire k-space is filled giving eight T2*-weighted images. The acquisition strategy is also sometimes referred to as an echo-planar-imaging (EPI) type readout. However, in the EPI sequence employed in functional brain studies, all the echoes acquired are assigned to the k-space matrix of a single image where the effective TE is the time at which the center of k-space is read. For cardiac applications, the sequence is cardiac-gated with the eight echoes acquired in the diastolic phase with 8-12 views per segment i.e. k-space lines per heartbeat.

Factors affecting measurement accuracy

There are a number of issues to consider in relation to measurement accuracy. One common source of error is RF pulse inhomogeneity. This refers to imperfections in the transmit field of the RF coil, which leads to certain locations in the imaging volume experiencing more or less RF power and, therefore, an imperfect RF flip angle for tipping magnetization and for refocusing. RF inhomogeneity affects all types of relaxation measurements. For T1 quantification, it represents the most common cause of errors and has an especially pronounced effect on the variable flip angle approach. To correct for this error, the most straight-forward solution is to map the RF B1 field to determine the true flip angles, and the correct flip angles can then be used in calculating relaxation times (108). For T2 quantification, RF inhomogeneity results in suboptimal refocusing pulses, which introduces T1-weighted stimulated echo pathways that interfere with the formation of pure spin-echoes for T2 measurement (117). This problem is more pronounced at 3 Tesla and higher, where fitting exponentials to the decay curves may not be appropriate. To achieve accurate T2 measurements, the stimulated echo problem needs to be addressed as described by Hennig (117) and in several recent reports (118,119).

Slice profile effects are another source of inaccuracy. Ideally, all the spins in the selected imaging slice should be inverted (in the case of a 180 degree pulse), and all spins outside the slice should remain unperturbed. In reality, the slice profile is never perfectly rectangular, which means that the actual flip angle falls off over a transition region at the edges of the slice. Hence,

the effective flip angle is not the nominal angle but is the integral of the inversion profile over the slice thickness. Slice profile imperfection affects both T1 and T2 measurements, even for gold standard measurements (120). This problem can be alleviated somewhat by using non-selective pulses or interleaving even and odd slices in a multislice slice-selective excitation.

Partial volume effects are a concern for all *in-vivo* experiments (121). This is especially problematic when different structures of interest all reside in close proximity in an imaging voxel. Examples include brain tissue (white and grey matter and CSF) and the interventricular septum (where the posterior segments are affected by susceptibility artifacts generated by the heart-lung interface and cardiac vein). Other sources of error include: magnetization transfer effects on T1 (122), exchange and diffusion effects on T2, temperature effects (T1 increases 2-3% per degree Celsius (64), and movement due to actual subject motion or bulk flow (e.g. blood flow) that artefactually shortens T1. Organ motion is especially problematic in body and cardiac applications. Breath-holding is an effective way to remove respiratory motion, but this is not feasible in some scenarios, such as in young children, where the only practical solution is to blur out motion artifacts by averaging (e.g. liver iron quantification) (123). Gating is another alternative to address respiratory motion. Organs with repetitive motion, such as the heart, can also utilize gating of data acquisitions. In organs where motion is not repetitive or predictable, one should use the most rapid methods possible for T1 and T2 mapping.

A final consideration to obtaining accurate measurements is having a good sense of target range of T1 or T2 values, because acquisition parameters (e.g. TR, TE, flip angles) can only be optimized for a limited range of relaxation times. For example, T2* accuracy depends critically on the minimum TE. For iron overload applications, T2* measurements should employ a minimum TE of at most 2 ms for most clinical cases (124). In the case of the liver, where iron stores can reach very high levels, even a TE of 0.8 ms, which corresponds to a maximum iron detection level of 40 mg/g dry tissue, is not adequate to quantify iron burdens as high as 60 mg/g that can occur in some patients.

Data fitting to extract relaxation parameters

To calculate relaxation times, the data acquired from the MRI experiment is fitted to some mathematical model. In many cases, the exponential function is used, as it describes many biophysical phenomena, including T1 and T2 relaxation. Estimation of T1 or T2 generally involves fitting a monoexponential function to the T1 or T2 relaxation curves. With conventional IR T1 measurement, an exponential fit to signal recovery at various TIs is performed. With spin-

echo (T2) or gradient-echo (T2*) measurements, an exponential fit to signal decay at various TEs is performed. In an ideal situation where there is no noise and there exists a single relaxation time in the imaging voxel, data fitting theoretically can be achieved using two data points on the monoexponential curve.

In the presence of noise, there is uncertainty in each measured data point. Hence, at least three data points need to be acquired, and there is also the question of how far apart they should be spaced to yield reliable estimates of T1, T2, or T2*. To improve quantitation accuracy, one may increase the number of measured data points, repeat the measurement at each data point to boost SNR, or combine both strategies. There is, however, a practical limit beyond which a greater number of measurements or averages will not yield additional benefit; the optimal balance between these two considerations can be determined through simulations. As a general rule, the lower and upper bounds of relaxation times to be measured are first identified. Then, for T2 or T2* measurement, the lowest TE at half the lower bound and the highest TE at twice the upper bound are chosen. Similarly, for T1 measurement, the lowest and highest TIs to include the lower and upper T1 bounds are chosen. These points can be equally spaced or logarithmically spaced. For a broader range of relaxation times expected, a higher number of data points is necessary. Once the required number of measurement points and their spacing are determined for modestly noisy data, further improvement in measurement accuracy should be reaped by repeating measurements to boost SNR, especially for the "noisy" data points.

However, the monoexponential model cannot describe all situations. It is valid only in an ideal situation where a single T1 or T2 relaxation time exists in an imaging voxel. This assumption may not hold in a number of situations. For instance, a single T1 assumption is valid in most tissues due to relatively fast water exchange amongst different compartments. However, when a high dose of contrast agent is present in the blood pool, exchange between the intra- and extra-vascular compartments is not necessarily fast and, thus, the effects of water exchange need to be considered. T2 decay may also deviate from a monoexponential model. For example, cartilage consists of several components (e.g. collagen and proteoglycans in the extracellular matrix) that have different influence on water, with the result that water may be tightly bound, more loosely bound, or freely moving. Only multicomponent T2 analysis can distinguish these components, as demonstrated in both cartilage (125) and collagen-based materials used for regeneration (53). Other models to describe T2 relaxation include: (1) non-exponential modeling of diffusion-mediated T2 relaxation, (2) chemical exchange, non-exponential or biexponential modeling of liver iron (126), and (3) biexponential modeling of blood oxygenation in muscle (127).

Multicomponent analysis, as alluded to above, refers to fitting multiple exponential components. In reality, a multitude of relaxation times associated with different tissue components always exists in an imaging voxel, but they generally cannot be resolved with the time scale of the MRI experiment. However, if exchange is slow compared to the relaxation time, then it is possible to differentiate distinct T1 and T2 components (128). For T1, multicomponent measurements are generally difficult to obtain, because exchange is fast compared to the T1 relaxation rate. On the other hand, multicomponent T2 analysis is much more common. For example, in the brain, T2 mapping experiments are assumed to be in the slow exchange regime; so, a multicomponent analysis differentiates at least two water compartments: intra/extracellular water and water trapped between the lipid bilayers of the myelin sheath. This is useful for measuring the myelin water fraction (MWF), which is a biomarker for myelin content. The most common acquisition sequence for multicomponent T2 measurement is based on the spin-echo (18). A more recent method is based on a SSFP sequence (129).

Once an appropriate model is chosen to describe relaxation, the method one adopts to perform the data fitting also affects measurement results. For example, in the analysis of multiexponential relaxation, there are a couple of approaches one can adopt: 1) assume the number of exponentials is known and fit to a model with a fixed number of exponentials, 2) use a non-negative least squares (NNLS) analysis that does not assume the number of exponentials is known. Although method 1 is easier to implement, method 2 is generally preferred, as it does not place any assumption on the nature of relaxation. Another example is fitting T2* data from iron overload patients (especially very high burdens). Here, constant offset correction is often used when fitting T2* signal decay to account for potential contributions from noise bias, heterogenous iron distribution in myocytes, analog-to-digital signal offsets, or contributions from iron-poor tissue such as fibroblasts, or myocardial blood volume (73). Some investigators truncate the TE echo points that are close to this 'noise floor' and fit only the remaining exponential part of the curve; this has been shown to provide better estimates when relaxation rates are low, however, the method is subjective.

DETAILED CASE STUDIES

Brain: Multiple Sclerosis

Multiple sclerosis lesions contain a large number of different pathologies, including demyelination, axonal loss and inflammation. The MS lesions are visible on T1- and T2-

weighted MRI scans, but these scans lack pathological specificity, making it difficult to differentiate pathologies and to track the evolution of the lesion from its acute gadolinium-enhancing stage through the process of remyelination. Recently, a number of quantitative MRI techniques have been proposed to study and track MS lesions. T1 and T2 mapping play a major role in these techniques, either as indirect myelin biomarkers, or as the foundation for more complex myelin models.

The myelin water fraction (MWF) is an indirect biomarker for myelin that is sensitive to the water trapped between the myelin sheaths. The restricted myelin water has short T2 values ($T2_{mw}$ ~ 10-50ms), whereas the free intra/extracellular water $T2_{ie}$ has values of 100ms or more. The myelin water fraction has been shown to decrease in MS lesions (18,130-132), as well as in normal appearing white matter (NAWM) in the brain (132) and spinal cord of MS patients (133). Figure 6 shows a myelin water fraction map, obtained from a 32-echo spin-echo sequence (19). The MWF exhibits good correlation with a luxol fast blue stain in gray matter, white matter and MS lesions.

Until recently, myelin water fraction maps were difficult to obtain in clinically feasible times, as the acquisition was restricted to a single slice and the scan time was prohibitively long. Recent work by Oh et al. has proposed multi-slice MWF mapping using a non-selective T2-prep sequence (134), while Deoni et al. have acquired MWF maps using steady state free precession (SSFP) techniques (129). These techniques are significantly faster than the conventional multi-echo spin-echo acquisition.

While myelin water fractions rely on computing the T2 relaxation time, T1 mapping can also play a roll in studying Gadolinium enhancing lesions, which appear as hyperintense on post-contrast T1-weighted scans. Figure 7 shows a longitudinal study tracking the T1 and T2 parameters in gadolinium-enhancing lesions up to 12 months after the lesions' appearance. In the figure, the T1 parameter has significantly higher values in the lesion compared to normal-appearing white matter (NAWM) and controls. This is most obvious at initial gadolinium enhancement, but it persists up to 12 months after presentation. At the same time, the T2 parameter is significantly increased. In the subsequent months, the relaxation parameters show recovery toward NAWM values, and the trends are consistent with the process of remyelination occurring in MS lesions.

T1 and T2 mapping also form the foundation of an advanced quantitative MRI technique called quantitative magnetization transfer (qMT). In qMT, the T1 and T2 parameters are entered in a two-pool tissue model that computes the semi-solid ratio (f), defined as the proportion of protons bound to macromolecules. In white matter, the semi-solid ratio has been shown to

correlate with myelin content, and it is particularly useful for characterizing the T1 black holes (135). Discussion of qMT is beyond the scope of this paper, but it provides an additional motivation for T1 and T2 quantification.

Body: Liver Iron

Clinical adoption of MRI relaxometry in the body is most evident for iron overload quantification, particularly in the liver where a diagnosis for total iron burden is made and the efficacy of chelation therapy determined. Recently, FDA approval was obtained for MRI liver iron assessment in place of biopsy for clinical diagnosis. The main impetus behind the successful clinical translation were the studies of St. Pierre et al. (41) and Wood et al. (136), which provided convincing liver-biopsy validation of non-invasive MRI measurements. Since that time, there has been a surge in MRI investigations for non-invasive iron quantification in the body. Quantifying iron overload in various disorders, particularly in transfusion-dependent thalassemia and in sickle-cell patients or those with deficient iron metabolism, and in different patient groups, including young children (137,138) and bone marrow transplants (139), has been reported. Figure 8 illustrates the use of rapid T2*-based MRI measurement of liver iron in a diverse pediatric population with iron overload disorders. The correlation obtained in these 151 children against gold-standard measurement is very high.

Another important objective from the perspective of patient management is to non-invasively monitor the effectiveness of iron chelation therapy. This requires that MRI be able to follow iron levels on an individual basis. In order to do so, several outstanding issues remain to be addressed. Measurements must be reproducible across different MRI scanners, as the same patient may be scanned on different platforms and at different field strengths throughout therapy. The mechanism by which a particular chelation therapy affects iron stores must also be understood as well as its relation to MRI relaxation times. It is unclear what differences to expect amongst different chelation therapies, but an initial step towards understanding the effect of iron distribution on calibrating MRI relaxations times was made recently in a simulation study (140). Finally, calibration curves remain to be established in other organs (e.g. pancreas, spleen) in order to broaden the clinical use of MRI for quantifying iron overload.

Cardiac: Acute Myocardial Infarction

Myocardial infarction typically occurs due to prolonged occlusion (> 30 min) of a major coronary artery, commonly referred to as a heart attack (141). While restoration of blood supply (reperfusion) is generally favorable following acute myocardial infarction in the heart (76), additional myocardial damage following reperfusion often presents itself as an adverse consequence (142). This is associated with an expansion of the prior ischemic damage resulting in greater cell death, edema (i.e. inflammation) and microvascular obstruction (MVO) or injury along with intramyocardial hemorrhage in the most severe cases (81). Quantitative relaxometry is well suited to detect some of these underlying remodeling processes given that relaxation times are modulated in different ways based the state of the tissue.

Figure 9 demonstrates T2 and T2* maps, along with early contrast enhanced (CE) short axis images in a porcine model of myocardial infarction in which the left anterior descending artery (LAD) was occluded for 90 min. followed by reperfusion (80). This model created large anteroseptal transmural infarcts characterized by MVO and hemorrhage; the pattern of progression of edema, hemorrhage and MVO are apparent in the images. Figure 10 (a, b) shows the cumulative time course of T2 and T2* relaxation parameters measured in the infarct and remote territories. In the infarct zone, T2 was significantly elevated beyond day 2 and remained elevated up to week 6 (Fig. 10a) suggesting that in severe infarcts, inflammatory response remains active even in the chronic stage. At day 2, histology revealed that both edema and hemorrhage were present in the infarct core and this is reflected by a T2 value that is not very different from control levels i.e. edema and hemorrhage have counter-acting effects on T2. On the other hand, T2* was more specific to hemorrhage (Fig. 10b) showing depressed values up to week 4; resolution of hemorrhage also coincided with resolution of MVO suggesting that the two phenomena are related. The hemorrhagic cores identified on T2* maps were typically with T2*<20 ms which is also the threshold used to detect myocardial iron overload (71).

Despite reperfusion therapy, microvascular integrity and function may be compromised in the infarcted as well as remote territories post-infarction (86). Myocardial BOLD imaging offers a novel means to examine myocardial perfusion reserve under pathologic conditions (89,143). Myocardial T2 and T2* values have been shown to increase in the stress state (pharmacological vasodilation); differences between rest and stress have been shown to reflect perfusion reserve. Figure 10 (c, d) shows the stress-induced effect on T2 post-AMI in the infarcted and remote myocardium. The infarct zone demonstrated a reduced/null hyperemic response indicative of damages and/or obstructed microvasculature; any residual response may

represent potentially salvageable myocardium. In remote myocardium, a subtle increase in resting T2 at week 1-2 might suggest either edema or hyperemia while the accompanied suppressed stress response might be indicative of a prior vasodilation or a resistive state arising from systemic inflammation or neurohormonal sympathetic activity.

Infarct remodeling post-ischemia is complex and the interaction between different pathophysiological mechanisms is not completely understood. Furthermore regional, serial and cross-subject monitoring of the remodeling processes is essential to understand the effects of novel therapies; for example, in addition to simply detecting (say) edema, it would be equally important to know the 'degree' of edema (i.e. lower or higher) in a particular treatment group. In this regard, quantitative relaxometry may be more specific than single images, providing a reliable and reproducible method to assess the inherent state of myocardial tissue *in vivo* following AMI.

DISCUSSION

As demonstrated in the various case studies, quantitative relaxation information extends MRI beyond anatomical mapping to characterization of the underlying pathophysiology in the tissue. Furthermore, the process of parameter estimation allows one to factor out hardware-driven fluctuations in signal intensity, notably those due to receive and transmit coil sensitivities, enabling focus on tissue characteristics. For instance, in the study of liver iron, biopsy is replaced with T2* measurement, getting detailed information about the physical amount of iron that is not accessible with conventional MRI. Indeed, this approach has numerous advantages over biopsy where one sparsely samples small tissue regions. Even exploratory surgery only reveals the characteristics of tissue surfaces. With relaxometry, spatial distributions of biological factors are obtained over a 3D volume in the body. Furthermore, with the characterization of multiple relaxation parameters (T1, T2, T2*), different properties of the tissue can be probed, yielding multiple degrees of freedom for differentiating various pathophysiological changes using more sophisticated image analysis tools such as statistical pattern recognition involving multiparamteric clustering and higher dimensional border determination.

These advantages of quantitation can be contrasted with qualitative assessment of tissue characteristics in single relaxometry-weighted images. In general, T1-, T2-, or T2*-weighted images are often considered more sensitive to disease (fewer false negatives) while relaxometry maps may be considered more specific (fewer false positives). That is, if the goal is to detect disease such as that associated with increased local deposition of iron, looking for local regions of

decreased signal in a T2*-weighted image may be particularly useful. However, many artifacts may also appear as iron deposits leading to an over-estimation of the extent of disease. With a map of T2* values, one can more accurately identify those regions containing higher iron concentrations and even estimate the local iron concentration.

The trade-off in performing quantitative measurements vs qualitative review of relaxometry-weighted images follows the traditional MRI trade-offs among imaging time, spatial resolution, and image quality as determined by signal-to-noise ratios (SNR). Quantitation requires the acquisition of multiple images to facilitate subsequent curve fitting, which is done at the expense of increasing the SNR or the resolution of a single relaxometry-weighted image. Furthermore, quantitation requires the alignment of the underlying images and makes assumptions about the nature of the signal behavior (e.g. exponential decay). Failure of these assumptions can introduce artifacts that can lead to misinterpretation.

How "good" the measurement of relaxation properties needs to be depends on the question being asked. In some cases, getting values that are accurate (i.e. consistent across individuals with the same underlying condition and across scanning platform) is less critical than getting values that are consistent within a given patient (i.e. the same for regions of similar pathology) and/or repeatable for the same patient with the same scanning set-up. Specifically, T1 maps following late gadolinium enhancement for cardiac scar assessment where the T1 values are consistent within a given scan would be sufficient for delineating scar volumes. Similarly, measuring repeatability (i.e. precision) is the greatest concern for longitudinal studies aimed at monitoring disease progression (e.g. comparison with MS studies tracking lesion evolution in a given subject over a period of 12 months) or therapeutic response (e.g. monitoring the effect of iron chelators on liver iron concentration in a given patient) if one can repeat the study with the same system.

Of course, measurement accuracy (consistency across patients and platforms) provides greater flexibility if it can be achieved. Notably, with accurate measurements, one could compare disease progression in different patients against a gold standard calibration performed in a select population. The capacity to compare measurements across patients also facilitates prediction of subsequent clinical outcomes and effectiveness of various therapies in particular patient groups. Accurate measurements also facilitate more specific assessment of magnitude of changes in underlying pathophysiology and comparison with target therapeutic endpoints (i.e. reduction of inflammation or iron concentration). Furthermore, one can develop more specific metrics for tissue classification if absolute relaxometry values reflecting various underlying physiological conditions are known from population studies.

CONCLUSION

Quantitative MRI opens up the possibility of measuring biophysical and physiological properties on an absolute level. Beyond the basic measurement of relaxation times as described in this review, other quantitative metrics can be derived, such as contrast dynamics related to vascular function, diffusion, spectroscopy, and magnetization transfer. Numerous other mechanisms that can potentially be quantified remain to be explored, and these may require incorporating intrinsic MRI parameters into complex tissue models. This review has described the key current clinical applications of MR relaxometry and provided a basic understanding of why different pathological conditions are best probed with specific MR parameters. Clinicians and researchers are encouraged to utilize the rich set of information available from MR relaxometry and to continue opening new frontiers for quantitative MRI.

ACKNOWLEDGEMENTS

REFERENCES

1. Bloembergen N, Purcell EM, Pound RV. Relaxation effects in nuclear magnetic resonance absorbtion. Phys Rev 1948;73:679.
2. Koenig SH, Brown RD, 3rd, Gibson JF, Ward RJ, Peters TJ. Relaxometry of ferritin solutions and the influence of the Fe3+ core ions. Magn Reson Med 1986;3(5):755-767.
3. Deoni S. Magnetic resonance relaxation and quantitative measurements in the brain. Magnetic Resonance Neuroimaging, Methods in Molecular Biology 2011;711:65-108.
4. Erkinjuntti T, Ketonen L, Sulkava R, Sipponen J, Vuorialho M, Iivanainen M. Do white matter changes on MRI and CT differentiate vascular dementia from Alzheimer's disease? J Neurol Neurosurg Psychiatry 1987;50(1):37-42.
5. Baudrexel S, Nurnberger L, Rub U, Seifried C, Klein JC, Deller T, Steinmetz H, Deichmann R, Hilker R. Quantitative mapping of T1 and T2* discloses nigral and brainstem pathology in early Parkinson's disease. Neuroimage 2010;51(2):512-520.
6. Haacke EM, Cheng NY, House MJ, Liu Q, Neelavalli J, Ogg RJ, Khan A, Ayaz M, Kirsch W, Obenaus A. Imaging iron stores in the brain using magnetic resonance imaging. Magn Reson Imaging 2005;23(1):1-25.
7. Quantitative MRI of the brain: measuring changes caused by disease. Tofts P, editor. Chichester, West Sussex: Wiley; 2005.
8. Miller DH, Grossman RI, Reingold SC, McFarland HF. The role of magnetic resonance techniques in understanding and managing multiple sclerosis. Brain 1998;121:3-24.
9. McDonald WI, Miller DH, Thompson AJ. Are magnetic resonance findings predictive of clinical outcome in therapeutic trials in multiple sclerosis? The dilemma of interferon-beta. Ann Neurol 1994;36(1):14-18.
10. Vrenken H, Geurts JJ, Knol DL, van Dijk LN, Dattola V, Jasperse B, van Schijndel RA, Polman CH, Castelijns JA, Barkhof F, Pouwels PJ. Whole-brain T1 mapping in multiple

sclerosis: global changes of normal-appearing gray and white matter. Radiology 2006;240(3):811-820.

11. Manfredonia F, Ciccarelli O, Khaleeli Z, Tozer DJ, Sastre-Garriga J, Miller DH, Thompson AJ. Normal-appearing brain t1 relaxation time predicts disability in early primary progressive multiple sclerosis. Arch Neurol 2007;64(3):411-415.

12. Papadopoulos K, Tozer DJ, Fisniku L, Altmann DR, Davies G, Rashid W, Thompson AJ, Miller DH, Chard DT. T1-relaxation time changes over five years in relapsing-remitting multiple sclerosis. Mult Scler 2010;16(4):427-433.

13. Bitsch A, Kuhlmann T, Stadelmann C, Lassmann H, Lucchinetti C, Bruck W. A longitudinal MRI study of histopathologically defined hypointense multiple sclerosis lesions. Ann Neurol 2001;49(6):793-796.

14. van Walderveen MA, Kamphorst W, Scheltens P, van Waesberghe JH, Ravid R, Valk J, Polman CH, Barkhof F. Histopathologic correlate of hypointense lesions on T1-weighted spin-echo MRI in multiple sclerosis. Neurology 1998;50(5):1282-1288.

15. Brix G, Schad LR, Deimling M, Lorenz WJ. Fast and precise T1 imaging using a TOMROP sequence. Magn Reson Imaging 1990;8(4):351-356.

16. Tardif CL, Collins DL, Eskildsen SF, Richardson JB, Pike GB. Segmentation of cortical MS lesions on MRI using automated laminar profile shape analysis. Med Image Comput Comput Assist Interv 2010;13(Pt 3):181-188.

17. Zellini F, Niepel G, Tench CR, Constantinescu CS. Hypothalamic involvement assessed by T1 relaxation time in patients with relapsing-remitting multiple sclerosis. Mult Scler 2009;15(12):1442-1449.

18. MacKay A, Whittall K, Adler J, Li D, Paty D, Graeb D. In vivo visualization of myelin water in brain by magnetic resonance. Magn Reson Med 1994;31(6):673-677.

19. Laule C, Leung E, Lis DK, Traboulsee AL, Paty DW, MacKay AL, Moore GR. Myelin water imaging in multiple sclerosis: quantitative correlations with histopathology. Mult Scler 2006;12(6):747-753.

20. MacKay AL, Vavasour IM, Rauscher A, Kolind SH, Madler B, Moore GR, Traboulsee AL, Li DK, Laule C. MR relaxation in multiple sclerosis. Neuroimaging Clin N Am 2009;19(1):1-26.

21. Ropele S, Langkammer C, Enzinger C, Fuchs S, Fazekas F. Relaxation time mapping in multiple sclerosis. Expert Rev Neurother 2011;11(3):441-450.

22. Englund E, Brun A, Gyorffy-Wagner Z, Larsson E, Persson B. Relaxation times in relation to grade of malignancy and tissue necrosis in astrocytic gliomas. Magn Reson Imag 1986;4:425-429.

23. Kurki T, Komu M. Spin-lattice relaxation and magnetization transfer in intracranial tumors in vivo: effects of Gd-DTPA on relaxation parameters. Magn Reson Imaging 1995;13(3):379-385.

24. Just M, Thelen M. Tissue characterization with T1, T2, and proton density values: results in 160 patients with brain tumors. Radiology 1988;169(3):779-785.

25. Tofts PS, Brix G, Buckley DL, Evelhoch JL, Henderson E, Knopp MV, Larsson HB, Lee TY, Mayr NA, Parker GJ, Port RE, Taylor J, Weisskoff RM. Estimating kinetic parameters from dynamic contrast-enhanced T(1)-weighted MRI of a diffusable tracer: standardized quantities and symbols. J Magn Reson Imaging 1999;10(3):223-232.

26. Sourbron S, Ingrisch M, Siefert A, Reiser M, Herrmann K. Quantification of cerebral blood flow, cerebral blood volume, and blood-brain-barrier leakage with DCE-MRI. Magn Reson Med 2009;62(1):205-217.

27. Runge VM, Muroff LR, Wells JW. Principles of contrast enhancement in the evaluation of brain diseases: an overview. J Magn Reson Imaging 1997;7(1):5-13.

28. Aronen HJ, Gazit IE, Louis DN, Buchbinder BR, Pardo FS, Weisskoff RM, Harsh GR, Cosgrove GR, Halpern EF, Hochberg FH, et al. Cerebral blood volume maps of gliomas: comparison with tumor grade and histologic findings. Radiology 1994;191(1):41-51.

29. Roberts HC, Roberts TP, Brasch RC, Dillon WP. Quantitative measurement of microvascular permeability in human brain tumors achieved using dynamic contrast-enhanced MR imaging: correlation with histologic grade. AJNR Am J Neuroradiol 2000;21(5):891-899.

30. DeWitt LD, Kistler JP, Miller DC, Richardson EP, Jr., Buonanno FS. NMR-neuropathologic correlation in stroke. Stroke 1987;18(2):342-351.

31. Bernarding J, Braun J, Hohmann J, Mansmann U, Hoehn-Berlage M, Stapf C, Wolf KJ, Tolxdorff T. Histogram-based characterization of healthy and ischemic brain tissues using multiparametric MR imaging including apparent diffusion coefficient maps and relaxometry. Magn Reson Med 2000;43(1):52-61.

32. Lansberg MG, Thijs VN, O'Brien MW, Ali JO, de Crespigny AJ, Tong DC, Moseley ME, Albers GW. Evolution of apparent diffusion coefficient, diffusion-weighted, and T2-weighted signal intensity of acute stroke. AJNR Am J Neuroradiol 2001;22(4):637-644.

33. Larsson HB, Hansen AE, Berg HK, Rostrup E, Haraldseth O. Dynamic contrast-enhanced quantitative perfusion measurement of the brain using T1-weighted MRI at 3T. J Magn Reson Imaging 2008;27(4):754-762.

34. Conlon P, Trimble MR, Rogers D, Callicott C. Magnetic resonance imaging in epilepsy: a controlled study. Epilepsy Res 1988;2(1):37-43.

35. Rugg-Gunn FJ, Boulby PA, Symms MR, Barker GJ, Duncan JS. Whole-brain T2 mapping demonstrates occult abnormalities in focal epilepsy. Neurology 2005;64(2):318-325.

36. Townsend TN, Bernasconi N, Pike GB, Bernasconi A. Quantitative analysis of temporal lobe white matter T2 relaxation time in temporal lobe epilepsy. Neuroimage 2004;23(1):318-324.

37. Baxendale SA, van Paesschen W, Thompson PJ, Connelly A, Duncan JS, Harkness WF, Shorvon SD. The relationship between quantitative MRI and neuropsychological functioning in temporal lobe epilepsy. Epilepsia 1998;39(2):158-166.

38. Van Paesschen W, Sisodiya S, Connelly A, Duncan JS, Free SL, Raymond AA, Grunewald RA, Revesz T, Shorvon SD, Fish DR, et al. Quantitative hippocampal MRI and intractable temporal lobe epilepsy. Neurology 1995;45(12):2233-2240.

39. Bernasconi A, Bernasconi N, Caramanos Z, Reutens DC, Andermann F, Dubeau F, Tampieri D, Pike BG, Arnold DL. T2 relaxometry can lateralize mesial temporal lobe epilepsy in patients with normal MRI. Neuroimage 2000;12(6):739-746.

40. Kaltwasser JP, Gottschalk R, Schalk KP, Hartl W. Non-invasive quantitation of liver iron-overload by magnetic resonance imaging. Br J Haematol 1990;74(3):360-363.

41. St Pierre TG, Clark PR, Chua-anusorn W, Fleming AJ, Jeffrey GP, Olynyk JK, Pootrakul P, Robins E, Lindeman R. Noninvasive measurement and imaging of liver iron concentrations using proton magnetic resonance. Blood 2005;105(2):855-861.

42. Wood JC, Enriquez C, Ghugre N, Otto-Duessel M, Aguilar M, Nelson MD, Moats R, Coates TD. Physiology and pathophysiology of iron cardiomyopathy in thalassemia. Ann N Y Acad Sci 2005;1054:386-395.

43. Papakonstantinou O, Alexopoulou E, Economopoulos N, Benekos O, Kattamis A, Kostaridou S, Ladis V, Efstathopoulos E, Gouliamos A, Kelekis NL. Assessment of iron distribution between liver, spleen, pancreas, bone marrow, and myocardium by means of R2 relaxometry with MRI in patients with beta-thalassemia major. J Magn Reson Imaging 2009;29(4):853-859.

44. Schwenzer NF, Machann J, Haap MM, Martirosian P, Schraml C, Liebig G, Stefan N, Haring HU, Claussen CD, Fritsche A, Schick F. T2* relaxometry in liver, pancreas, and spleen in a healthy cohort of one hundred twenty-nine subjects-correlation with age, gender, and serum ferritin. Invest Radiol 2008;43(12):854-860.

45. Schein A, Enriquez C, Coates TD, Wood JC. Magnetic resonance detection of kidney iron deposition in sickle cell disease: a marker of chronic hemolysis. J Magn Reson Imaging 2008;28(3):698-704.

46. Berdoukas V, Chouliaras G, Moraitis P, Zannikos K, Berdoussi E, Ladis V. The efficacy of iron chelator regimes in reducing cardiac and hepatic iron in patients with thalassaemia major: a clinical observational study. J Cardiovasc Magn Reson 2009;11:20.

47. Recht MP, Resnick D. Magnetic resonance imaging of articular cartilage: an overview. Top Magn Reson Imaging 1998;9(6):328-336.

48. Link TM, Stahl R, Woertler K. Cartilage imaging: motivation, techniques, current and future significance. Eur Radiol 2007;17(5):1135-1146.

49. Blumenkrantz G, Majumdar S. Quantitative magnetic resonance imaging of articular cartilage in osteoarthritis. Eur Cell Mater 2007;13:76-86.

50. Williams A, Gillis A, McKenzie C, Po B, Sharma L, Micheli L, McKeon B, Burstein D. Glycosaminoglycan distribution in cartilage as determined by delayed gadolinium-enhanced MRI of cartilage (dGEMRIC): potential clinical applications. AJR Am J Roentgenol 2004;182(1):167-172.

51. Eckstein F, Burstein D, Link TM. Quantitative MRI of cartilage and bone: degenerative changes in osteoarthritis. NMR Biomed 2006;19(7):822-854.

52. Kight AC, Dardzinski BJ, Laor T, Graham TB. Magnetic resonance imaging evaluation of the effects of juvenile rheumatoid arthritis on distal femoral weight-bearing cartilage. Arthritis Rheum 2004;50(3):901-905.

53. Cheng HL, Islam SS, Loai Y, Antoon R, Beaumont M, Farhat WA. Quantitative magnetic resonance imaging assessment of matrix development in cell-seeded natural urinary bladder smooth muscle tissue-engineered constructs. Tissue Eng Part C Methods 2010;16(4):643-651.

54. Stikov N, Keenan KE, Pauly JM, Smith RL, Dougherty RF, Gold GE. Cross-relaxation imaging of human articular cartilage. Magn Reson Med 2011;66(3):725-734.

55. Potter HG, Chong le R, Sneag DB. Magnetic resonance imaging of cartilage repair. Sports Med Arthrosc 2008;16(4):236-245.

56. Chai JW, Lin YC, Chen JH, Wu CC, Lee CP, Chu WC, Lee SK. In vivo magnetic resonance (MR) study of fatty liver: importance of intracellular ultrastructural alteration for MR tissue parameters change. J Magn Reson Imaging 2001;14(1):35-41.

57. de Miguel MH, Yeung HN, Goyal M, Noh JW, Aisen AM, Phan SH, Wiggins RC. Evaluation of quantitative magnetic resonance imaging as a noninvasive technique for measuring renal scarring in a rabbit model of antiglomerular basement membrane disease. J Am Soc Nephrol 1994;4(11):1861-1868.

58. Johnson K, Davis PJ, Foster JK, McDonagh JE, Ryder CA, Southwood TR. Imaging of muscle disorders in children. Pediatr Radiol 2006;36(10):1005-1018.

59. Maillard SM, Jones R, Owens C, Pilkington C, Woo P, Wedderburn LR, Murray KJ. Quantitative assessment of MRI T2 relaxation time of thigh muscles in juvenile dermatomyositis. Rheumatology (Oxford) 2004;43(5):603-608.

60. Workie DW, Graham TB, Laor T, Rajagopal A, O'Brien KJ, Bommer WA, Racadio JM, Shire NJ, Dardzinski BJ. Quantitative MR characterization of disease activity in the knee in children with juvenile idiopathic arthritis: a longitudinal pilot study. Pediatr Radiol 2007;37(6):535-543.

61. Verstraete KL, Lang P. Bone and soft tissue tumors: the role of contrast agents for MR imaging. Eur J Radiol 2000;34(3):229-246.

62. Gambarota G, Veltien A, van Laarhoven H, Philippens M, Jonker A, Mook OR, Frederiks WM, Heerschap A. Measurements of T1 and T2 relaxation times of colon cancer metastases in rat liver at 7 T. Magma 2004;17(3-6):281-287.

63. Cieszanowski A, Szeszkowski W, Golebiowski M, Bielecki DK, Grodzicki M, Pruszynski B. Discrimination of benign from malignant hepatic lesions based on their T2-relaxation times calculated from moderately T2-weighted turbo SE sequence. Eur Radiol 2002;12(9):2273-2279.

64. Rieke V, Butts Pauly K. MR thermometry. J Magn Reson Imaging 2008;27(2):376-390.

65. Winter JD, Estrada M, Cheng HL. Normal tissue quantitative T1 and T2* MRI relaxation time responses to hypercapnic and hyperoxic gases. Acad Radiol 2011;18(9):1159-1167.

66. Rhee TK, Larson AC, Prasad PV, Santos E, Sato KT, Salem R, Deng J, Paunesku T, Woloschak GE, Mulcahy MF, Li D, Omary RA. Feasibility of blood oxygenation level-dependent MR imaging to monitor hepatic transcatheter arterial embolization in rabbits. J Vasc Interv Radiol 2005;16(11):1523-1528.

67. Dyke JP, Panicek DM, Healey JH, Meyers PA, Huvos AG, Schwartz LH, Thaler HT, Tofts PS, Gorlick R, Koutcher JA, Ballon D. Osteogenic and Ewing sarcomas: estimation of necrotic fraction during induction chemotherapy with dynamic contrast-enhanced MR imaging. Radiology 2003;228(1):271-278.

68. Krasin MJ, Xiong X, Reddick WE, Ogg RJ, Hoffer FA, McCarville B, Kaste SC, Spunt SL, Navid F, Davidoff AM, Zhang L, Kun LE, Merchant TE. A model for quantitative changes in the magnetic resonance parameters of muscle in children after therapeutic irradiation. Magn Reson Imaging 2006;24(10):1319-1324.

69. Andersson T, Ericsson A, Eriksson B, Hemmingsson A, Lindh E, Nyman R, Oberg K. Relative proton density and relaxation times in liver metastases during interferon treatment. Br J Radiol 1989;62(737):433-437.

70. Stoffner R, Schullian P, Widmann G, Bale R, Kremser C. [Magnetic resonance imaging of radiofrequency current-induced coagulation zones in the ex vivo bovine liver]. Rofo 2010;182(8):690-697.

71. Anderson LJ, Holden S, Davis B, Prescott E, Charrier CC, Bunce NH, Firmin DN, Wonke B, Porter J, Walker JM, Pennell DJ. Cardiovascular T2-star (T2*) magnetic resonance for the early diagnosis of myocardial iron overload. Eur Heart J 2001;22(23):2171-2179.

72. Carpenter JP, He T, Kirk P, Roughton M, Anderson LJ, de Noronha SV, Sheppard MN, Porter JB, Walker JM, Wood JC, Galanello R, Forni G, Catani G, Matta G, Fucharoen S, Fleming A, House MJ, Black G, Firmin DN, St Pierre TG, Pennell DJ. On T2* magnetic resonance and cardiac iron. Circulation 2011;123(14):1519-1528.

73. Ghugre NR, Enriquez CM, Gonzalez I, Nelson MD, Jr., Coates TD, Wood JC. MRI detects myocardial iron in the human heart. Magn Reson Med 2006;56(3):681-686.

74. Wood JC, Otto-Duessel M, Gonzalez I, Aguilar MI, Shimada H, Nick H, Nelson M, Moats R. Deferasirox and deferiprone remove cardiac iron in the iron-overloaded gerbil. Transl Res 2006;148(5):272-280.

75. Wood JC, Aguilar M, Otto-Duessel M, Nick H, Nelson MD, Moats R. Influence of iron chelation on R1 and R2 calibration curves in gerbil liver and heart. Magn Reson Med 2008;60(1):82-89.

76. Van de Werf F, Bax J, Betriu A, Blomstrom-Lundqvist C, Crea F, Falk V, Filippatos G, Fox K, Huber K, Kastrati A, Rosengren A, Steg PG, Tubaro M, Verheugt F, Weidinger F, Weis M. Management of acute myocardial infarction in patients presenting with persistent ST-segment elevation: the Task Force on the Management of ST-Segment Elevation Acute Myocardial Infarction of the European Society of Cardiology. Eur Heart J 2008;29(23):2909-2945.

77. Bradley WG, Jr. MR appearance of hemorrhage in the brain. Radiology 1993;189(1):15-26.

78. Friedrich MG, Abdel-Aty H, Taylor A, Schulz-Menger J, Messroghli D, Dietz R. The salvaged area at risk in reperfused acute myocardial infarction as visualized by cardiovascular magnetic resonance. J Am Coll Cardiol 2008;51(16):1581-1587.

79. Giri S, Chung YC, Merchant A, Mihai G, Rajagopalan S, Raman SV, Simonetti OP. T2 quantification for improved detection of myocardial edema. J Cardiovasc Magn Reson 2009;11(1):56.

80. Ghugre NR, Ramanan V, Pop M, Yang Y, Barry J, Qiang B, Connelly KA, Dick AJ, Wright GA. Quantitative tracking of edema, hemorrhage, and microvascular obstruction in subacute myocardial infarction in a porcine model by MRI. Magn Reson Med 2011;66(4):1129-1141.

81. Ganame J, Messalli G, Dymarkowski S, Rademakers FE, Desmet W, Van de Werf F, Bogaert J. Impact of myocardial haemorrhage on left ventricular function and remodelling in patients with reperfused acute myocardial infarction. Eur Heart J 2009;30(12):1440-1449.

82. Garcia-Dorado D, Theroux P, Solares J, Alonso J, Fernandez-Aviles F, Elizaga J, Soriano J, Botas J, Munoz R. Determinants of hemorrhagic infarcts. Histologic observations from experiments involving coronary occlusion, coronary reperfusion, and reocclusion. Am J Pathol 1990;137(2):301-311.

83. Lotan CS, Miller SK, Bouchard A, Cranney GB, Reeves RC, Bishop SP, Elgavish GA, Pohost GM. Detection of intramyocardial hemorrhage using high-field proton (1H) nuclear magnetic resonance imaging. Cathet Cardiovasc Diagn 1990;20(3):205-211.

84. Leung G, Moody AR. MR imaging depicts oxidative stress induced by methemoglobin. Radiology 2010;257(2):470-476.

85. Foltz WD, Yang Y, Graham JJ, Detsky JS, Wright GA, Dick AJ. MRI relaxation fluctuations in acute reperfused hemorrhagic infarction. Magn Reson Med 2006;56(6):1311-1319.

86. Uren NG, Crake T, Lefroy DC, de Silva R, Davies GJ, Maseri A. Reduced coronary vasodilator function in infarcted and normal myocardium after myocardial infarction. N Engl J Med 1994;331(4):222-227.

87. Wacker CM, Bock M, Hartlep AW, Beck G, van Kaick G, Ertl G, Bauer WR, Schad LR. Changes in myocardial oxygenation and perfusion under pharmacological stress with dipyridamole: assessment using T*2 and T1 measurements. Magn Reson Med 1999;41(4):686-695.

88. Foltz WD, Huang H, Fort S, Wright GA. Vasodilator response assessment in porcine myocardium with magnetic resonance relaxometry. Circulation 2002;106(21):2714-2719.

89. Ghugre NR, Ramanan V, Pop M, Yang Y, Barry J, Qiang B, Connelly KA, Dick AJ, Wright GA. Myocardial BOLD imaging at 3 T using quantitative T2: application in a myocardial infarct model. Magn Reson Med 2011;66(6):1739-1747.

90. Yan AT, Shayne AJ, Brown KA, Gupta SN, Chan CW, Luu TM, Di Carli MF, Reynolds HG, Stevenson WG, Kwong RY. Characterization of the peri-infarct zone by contrast-enhanced cardiac magnetic resonance imaging is a powerful predictor of post-myocardial infarction mortality. Circulation 2006;114(1):32-39.

91. Schmidt A, Azevedo CF, Cheng A, Gupta SN, Bluemke DA, Foo TK, Gerstenblith G, Weiss RG, Marban E, Tomaselli GF, Lima JA, Wu KC. Infarct tissue heterogeneity by magnetic resonance imaging identifies enhanced cardiac arrhythmia susceptibility in patients with left ventricular dysfunction. Circulation 2007;115(15):2006-2014.

92. Messroghli DR, Greiser A, Frohlich M, Dietz R, Schulz-Menger J. Optimization and validation of a fully-integrated pulse sequence for modified look-locker inversion-

recovery (MOLLI) T1 mapping of the heart. J Magn Reson Imaging 2007;26(4):1081-1086.

93. Detsky JS, Paul G, Dick AJ, Wright GA. Reproducible classification of infarct heterogeneity using fuzzy clustering on multicontrast delayed enhancement magnetic resonance images. IEEE Trans Med Imaging 2009;28(10):1606-1614.

94. Jackowski C, Christe A, Sonnenschein M, Aghayev E, Thali MJ. Postmortem unenhanced magnetic resonance imaging of myocardial infarction in correlation to histological infarction age characterization. Eur Heart J 2006;27(20):2459-2467.

95. Waller C, Kahler E, Hiller KH, Hu K, Nahrendorf M, Voll S, Haase A, Ertl G, Bauer WR. Myocardial perfusion and intracapillary blood volume in rats at rest and with coronary dilatation: MR imaging in vivo with use of a spin-labeling technique. Radiology 2000;215(1):189-197.

96. Vignaux O, Dhote R, Duboc D, Blanche P, Dusser D, Weber S, Legmann P. Clinical significance of myocardial magnetic resonance abnormalities in patients with sarcoidosis: a 1-year follow-up study. Chest 2002;122(6):1895-1901.

97. Abdel-Aty H, Simonetti O, Friedrich MG. T2-weighted cardiovascular magnetic resonance imaging. J Magn Reson Imaging 2007;26(3):452-459.

98. Aherne T, Yee ES, Tscholakoff D, Gollin G, Higgins C, Ebert PA. Diagnosis of acute and chronic cardiac rejection by magnetic resonance imaging: a non-invasive in-vivo study. J Cardiovasc Surg (Torino) 1988;29(5):587-590.

99. Conrad CH, Brooks WW, Hayes JA, Sen S, Robinson KG, Bing OH. Myocardial fibrosis and stiffness with hypertrophy and heart failure in the spontaneously hypertensive rat. Circulation 1995;91(1):161-170.

100. Mewton N, Liu CY, Croisille P, Bluemke D, Lima JA. Assessment of myocardial fibrosis with cardiovascular magnetic resonance. J Am Coll Cardiol 2011;57(8):891-903.

101. Barral JK, Gudmundson E, Stikov N, Etezadi-Amoli M, Stoica P, Nishimura DG. A robust methodology for in vivo T1 mapping. Magn Reson Med 2011;64(4):1057-1067.

102. Zhu DC, Penn RD. Full-brain T1 mapping through inversion recovery fast spin echo imaging with time-efficient slice ordering. Magn Reson Med 2005;54(3):725-731.

103. Gowland PA, Leach MO. A simple method for the restoration of signal polarity in multi-image inversion recovery sequences for measuring T1. Magn Reson Med 1991;18(1):224-231.

104. Look DC, Locker DR. Time saving in measurement of NMR and EPR relaxation times. Rev Sci Instrum 1970;41(2):250-251.

105. Messroghli DR, Radjenovic A, Kozerke S, Higgins DM, Sivananthan MU, Ridgway JP. Modified Look-Locker inversion recovery (MOLLI) for high-resolution T1 mapping of the heart. Magn Reson Med 2004;52(1):141-146.

106. Slavin GS, Gupta SN. Efficient T1 mapping of the heart using an interleaved look-locker acquisition with saturation recovery. SCMR 2007: February 2-4, Rome, Italy 2007:Abs. 324.

107. Deoni SC, Rutt BK, Peters TM. Rapid combined T1 and T2 mapping using gradient recalled acquisition in the steady state. Magn Reson Med 2003;49(3):515-526.

108. Cheng HL, Wright GA. Rapid high-resolution T(1) mapping by variable flip angles: accurate and precise measurements in the presence of radiofrequency field inhomogeneity. Magn Reson Med 2006;55(3):566-574.

109. Kershaw LE, Cheng HL. A general dual-bolus approach for quantitative DCE-MRI. Magn Reson Imaging 2011;29(2):160-166.

110. Winter JD, Akens MK, Cheng HL. Quantitative MRI assessment of VX2 tumour oxygenation changes in response to hyperoxia and hypercapnia. Phys Med Biol 2011;56(5):1225-1242.

111. Winter JD, St Lawrence KS, Margaret Cheng HL. Quantification of renal perfusion: Comparison of arterial spin labeling and dynamic contrast-enhanced MRI. J Magn Reson Imaging Jul 14 (Epub ahead of print) 2011.

112. Whittall KP, MacKay AL, Graeb DA, Nugent RA, Li DK, Paty DW. In vivo measurement of T2 distributions and water contents in normal human brain. Magn Reson Med 1997;37(1):34-43.

113. Sussman MS, Vidarsson L, Pauly JM, Cheng HL. A technique for rapid single-echo spin-echo T2 mapping. Magn Reson Med 2010;64(2):536-545.

114. Deoni SC, Ward HA, Peters TM, Rutt BK. Rapid T2 estimation with phase-cycled variable nutation steady-state free precession. Magn Reson Med 2004;52(2):435-439.

115. Brittain JH, Hu BS, Wright GA, Meyer CH, Macovski A, Nishimura DG. Coronary angiography with magnetization-prepared T2 contrast. Magn Reson Med 1995;33(5):689-696.

116. Zia M, Ghugre N, Paul G, Stainsby J, Ramanan V, Connelly K, Wright G, Dick A. Characterizing myocardial edema and hemorrhage using T2, T2*, and diastolic wall thickness post acute myocardial infarction. Journal of Cardiovascular Magnetic Resonance 2010;12(Suppl 1):P179.

117. Hennig J. Multiecho imaging sequences with low refocusing flip angles. J Magn Reson 1988;78(3):397-407.

118. Lebel RM, Wilman AH. Transverse relaxometry with stimulated echo compensation. Magn Reson Med;64(4):1005-1014.

119. Prasloski T, Madler B, Xiang QS, Mackay A, Jones C. Applications of stimulated echo correction to multicomponent T(2) analysis. Magn Reson Med, Oct 19 doi: 101002/mrm23157 2011.

120. Kingsley PB, Ogg RJ, Reddick WE, Steen RG. Correction of errors caused by imperfect inversion pulses in MR imaging measurement of T1 relaxation times. Magn Reson Imaging 1998;16(9):1049-1055.

121. Rakow-Penner R, Daniel B, Yu H, Sawyer-Glover A, Glover GH. Relaxation times of breast tissue at 1.5T and 3T measured using IDEAL. J Magn Reson Imaging 2006;23(1):87-91.

122. Gochberg DF, Gore JC. Quantitative magnetization transfer imaging via selective inversion recovery with short repetition times. Magn Reson Med 2007;57(2):437-441.

123. Beaumont M, Odame I, Babyn PS, Vidarsson L, Kirby-Allen M, Cheng HL. Accurate liver T2 measurement of iron overload: a simulations investigation and in vivo study. J Magn Reson Imaging 2009;30(2):313-320.

124. Ghugre NR, Enriquez CM, Coates TD, Nelson MD, Jr., Wood JC. Improved R2* measurements in myocardial iron overload. J Magn Reson Imaging 2006;23(1):9-16.

125. Reiter D, Roque R, Lin P, Irrechukwu O, Doty S, Longo D, Pleshko N, Spencer R. Mapping proteoglycan-bound water in cartilage: Improved specificity of matrix assessment using multiexponential transverse relaxation analysis. Magn Reson Med 2011;65(2):377-384.

126. Ghugre NR, Coates TD, Nelson MD, Wood JC. Mechanisms of tissue-iron relaxivity: nuclear magnetic resonance studies of human liver biopsy specimens. Magn Reson Med 2005;54(5):1185-1193.

127. Noseworthy MD, Kim JK, Stainsby JA, Stanisz GJ, Wright GA. Tracking oxygen effects on MR signal in blood and skeletal muscle during hyperoxia exposure. J Magn Reson Imaging 1999;9(6):814-820.

128. Zimmerman J, Britten W. Nuclear magnetic resonance studies in multiple phase systems: lifetimes of a water molecule in an absorbing phase silica gel. J Phys Chem 1957;61(1328).

129. Deoni SC, Rutt BK, Arun T, Pierpaoli C, Jones DK. Gleaning multicomponent T1 and T2 information from steady-state imaging data. Magn Reson Med 2008;60(6):1372-1387.

130. Tozer DJ, Davies GR, Altmann DR, Miller DH, Tofts PS. Correlation of apparent myelin measures obtained in multiple sclerosis patients and controls from magnetization transfer and multicompartmental T2 analysis. Magn Reson Med 2005;53(6):1415-1422.

131. Vavasour IM, Whittall KP, MacKay AL, Li DK, Vorobeychik G, Paty DW. A comparison between magnetization transfer ratios and myelin water percentages in normals and multiple sclerosis patients. Magn Reson Med 1998;40(5):763-768.

132. Laule C, Vavasour IM, Moore GR, Oger J, Li DK, Paty DW, MacKay AL. Water content and myelin water fraction in multiple sclerosis. A T2 relaxation study. J Neurol 2004;251(3):284-293.

133. Wu Y, Alexander AL, Fleming JO, Duncan ID, Field AS. Myelin water fraction in human cervical spinal cord in vivo. J Comput Assist Tomogr 2006;30(2):304-306.

134. Oh J, Han ET, Pelletier D, Nelson SJ. Measurement of in vivo multi-component T2 relaxation times for brain tissue using multi-slice T2 prep at 1.5 and 3 T. Magn Reson Imaging 2006;24(1):33-43.

135. Levesque I, Sled JG, Narayanan S, Santos AC, Brass SD, Francis SJ, Arnold DL, Pike GB. The role of edema and demyelination in chronic T1 black holes: a quantitative magnetization transfer study. J Magn Reson Imaging 2005;21(2):103-110.

136. Wood JC, Enriquez C, Ghugre N, Tyzka JM, Carson S, Nelson MD, Coates TD. MRI R2 and R2* mapping accurately estimates hepatic iron concentration in transfusion-dependent thalassemia and sickle cell disease patients. Blood 2005;106(4):1460-1465.

137. Argyropoulou MI, Kiortsis DN, Astrakas L, Metafratzi Z, Chalissos N, Efremidis SC. Liver, bone marrow, pancreas and pituitary gland iron overload in young and adult thalassemic patients: a T2 relaxometry study. Eur Radiol 2007;17(12):3025-3030.

138. Cheng HL, Holowka S, Moineddin R, Odame I. Liver iron overload assessment by T2* magnetic resonance imaging in pediatric patients: an accuracy and reproducibility study. Am J Hematol (in press) 2012.

139. Kornreich L, Horev G, Yaniv I, Stein J, Grunebaum M, Zaizov R. Iron overload following bone marrow transplantation in children: MR findings. Pediatr Radiol 1997;27(11):869-872.

140. Ghugre NR, Wood JC. Relaxivity-iron calibration in hepatic iron overload: Probing underlying biophysical mechanisms using a Monte Carlo model. Magn Reson Med 2011;65(3):837-847.

141. Reimer KA, Lowe JE, Rasmussen MM, Jennings RB. The wavefront phenomenon of ischemic cell death. 1. Myocardial infarct size vs duration of coronary occlusion in dogs. Circulation 1977;56(5):786-794.

142. Yellon DM, Hausenloy DJ. Myocardial reperfusion injury. N Engl J Med 2007;357(11):1121-1135.

143. Dharmakumar R, Arumana JM, Tang R, Harris K, Zhang Z, Li D. Assessment of regional myocardial oxygenation changes in the presence of coronary artery stenosis with balanced SSFP imaging at 3.0 T: theory and experimental evaluation in canines. J Magn Reson Imaging 2008;27(5):1037-1045.

FIGURE LEGENDS

Figure 1: A schematic of T1 mapping sequences: a) Inversion Recovery, b) Look-Locker, c) Variable Flip Angle.

Figure 2: A schematic of an inversion recovery sequence (top) and the T1 relaxation curve (bottom). The relaxation curve is sampled at several points TI, and then fitted to a single exponential.

Figure 3: A schematic of a multi-echo spin echo sequence (top) and the T2 relaxation curve (bottom). The relaxation curve is sampled at several points TE, and then fitted to a single exponential with a relaxation time T2.

Figure 4: (a) Typical spin echo sequence for T2 measurement. (b) Magnetization preparation where T2-weighted contrast is prepared in advance of excitation and readout. (c) Example of a sequence using T2-preparation with a spectro-spatial RF excitation and spiral readout; TE is determined by the number of 180 refocussing pulses.

Figure 5: Multi-echo gradient echo sequence with echo-planar-imaging (EPI-type) readout for the measurement of T2*. Eight echos are typically acquired ranging from 2-15 ms with TR=20 ms. The free-induction-decay (FID) is shown with exponential time constant T2*.

Figure 6: (Top) Example of a 7.0 T TE = 20.1 ms image and myelin water fraction (MWF) map and corresponding luxol fast blue histology image of the parieto-occipital region of a patient who has MS. A good qualitative correspondence is observed between the MWF map and histology stain for myelin. The normal prominent myelination of the deeper cortical layers (arrows) is also visible on the myelin water image. (Bottom) Examples of the quantitative correlation between myelin water fraction (MWF) and luxol fast blue optical density (LFB OD) for gray matter (GM), lesion, dirty-appearing white matter (DAWM), and normal appearing white matter (NAWM) for two MS samples (from MacKay et al. MR Relaxation in Multiple Sclerosis Nueroimag Clin N Am 19 (2009) 1-26; with permission).

Figure 7. a) Initial post-Gd T1-weighted scan of a single patient with outlines of enhancing region (green) and contralateral NAWM (cyan) b) T1 map of the same subject (units are s) c) Plot

of T1, averaged across five subjects at 8 time-points distributed over 12 months, starting at initial Gd enhancement. Error bars indicate the standard error of the mean across subjects d) T2-weighted image resampled to the lower resolution of the quantitative maps e) T2 map of the same subject (units are s) f) Plot of T2, averaged across five subjects at 8 time-points distributed over 12 months, starting at initial Gd enhancement. Error bars indicate the standard error of the mean across subjects (adapted from Levesque et al. Magn Reson Med, 2010, 63:633-640; with permission). Gd = Gadolinium.

Figure 8: Absolute liver iron measurement in children. (a) Coronal image slice showing the T2* relaxation time distribution in the liver of a patient with iron overload. Red outline was manually drawn to contour the liver. (b) Measured absolute liver iron from T2* relaxation times compared against reference measurements in 151 pediatric patients ($r = 0.94$). Line of identity is shown.

Figure 9: Longitudinal changes in edema, hemorrhage and MVO. T2 and T2* maps are shown along with early contrast enhanced (CE) images at various time points post-AMI in a porcine model of myocardial infarction. ***Day 2:*** T2 elevation usually associated with edema was not apparent in the infarct zone (39.2 ms vs. 39.1 ms control) but T2 was slightly elevated in the peripheral areas; Arrows indicate focal signal-void regions or T2* abnormalities (18.5 ms vs. 34.2 ms control) within the MVO as delineated by the CE image. ***Week 1:*** T2 was elevated (arrows) in most of the infarct (51.1 ms) with reduced sub-endocardial T2* (15.8 ms) indicative of diffuse hemorrhagic by-products (arrows). ***Week 4:*** T2 was still elevated (50 ms) while normalization of T2* (35 ms) coincided with resolution of MVO. (Reproduced from Ghugre et al., Magn Reson Med, 2011, 66(4): 1129-41; with permission).

Figure 10: Quantitative fluctuations in relaxation parameters after AMI. Plots (a) and (b) demonstrate longitudinal fluctuations in T2 and T2* in the infarct zone compared to remote myocardium averaged over all animals; day 0 represents values from healthy controls and error bars represent standard error. Plots (c) and (d) show evolution of T2 in the rest and stress states (dipyridamole induced pharmacological vasodilation) in infarcted and remote myocardium, respectively; the difference between the two states is a reflection of vasodilaory function or myocardial perfusion reserve. † $p<0.05$, compared to control values; § $p<0.05$, compared to the previous time point; ¶ $p<0.05$ compared to rest values. (Modified from Ghugre et al., Magn Reson Med 2011, 66(4): 1129-41 and Ghugre et al., Magn Reson Med, 2011, 66(6):1739-1747; with permission).

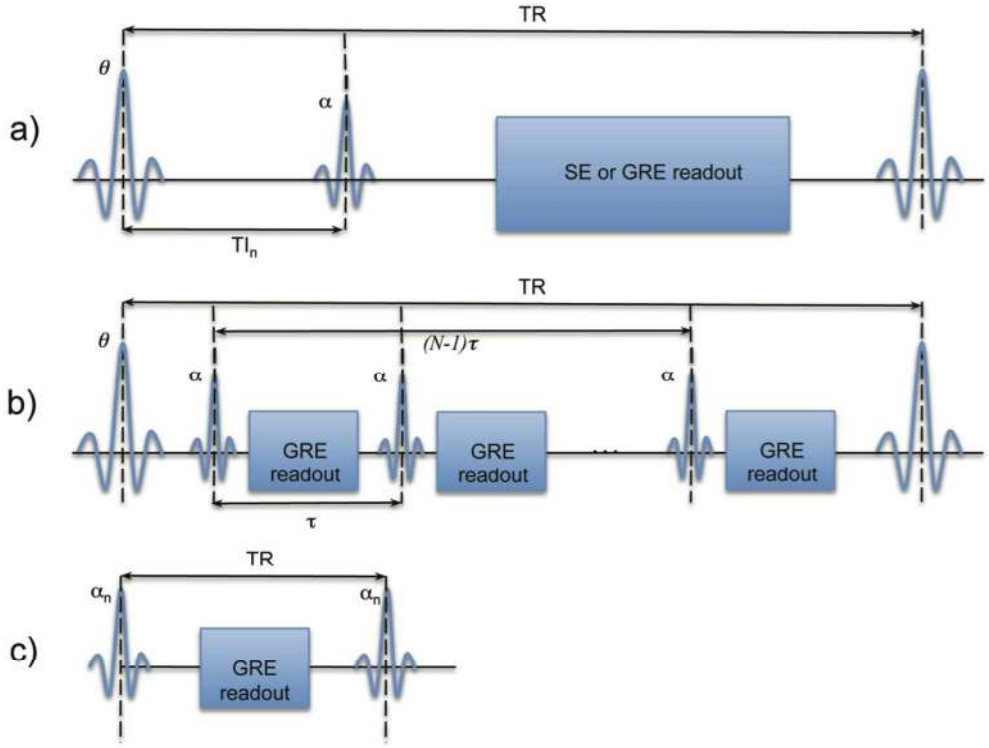

Figure 1: A schematic of T1 mapping sequences: a) Inversion Recovery, b) Look-Locker, c) Variable Flip Angle.
143x109mm (300 x 300 DPI)

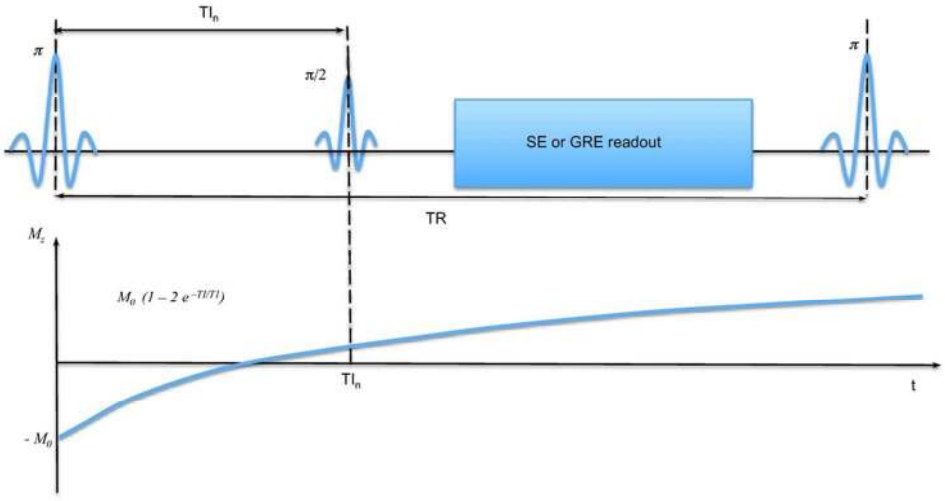

Figure 2: A schematic of an inversion recovery sequence (top) and the T1 relaxation curve (bottom). The relaxation curve is sampled at several points TI, and then fitted to a single exponential.
100x50mm (300 x 300 DPI)

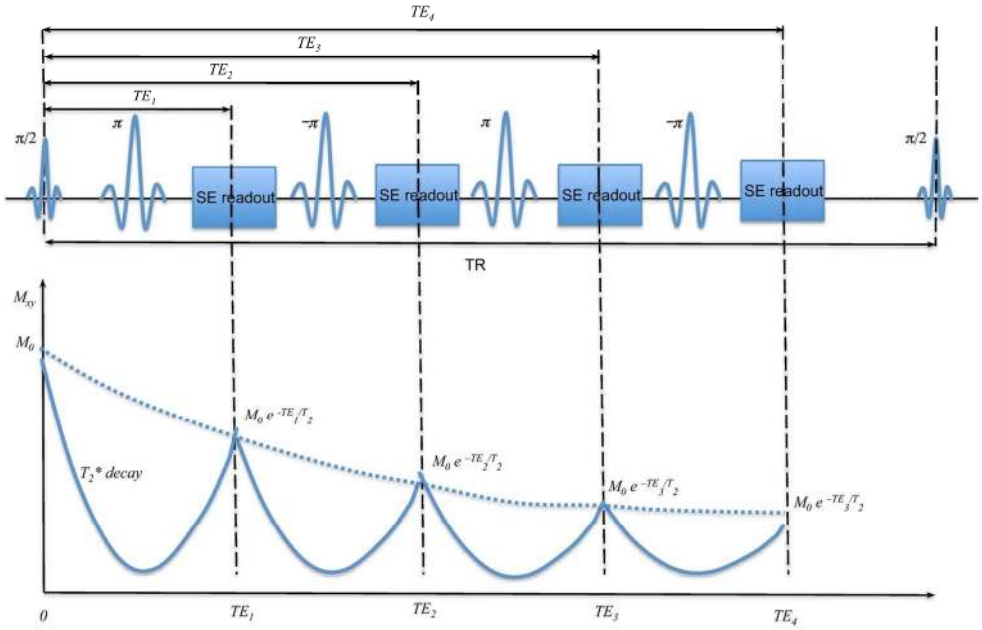

Figure 3: A schematic of a multi-echo spin echo sequence (top) and the T2 relaxation curve (bottom). The relaxation curve is sampled at several points TE, and then fitted to a single exponential with a relaxation time T2.
127x80mm (300 x 300 DPI)

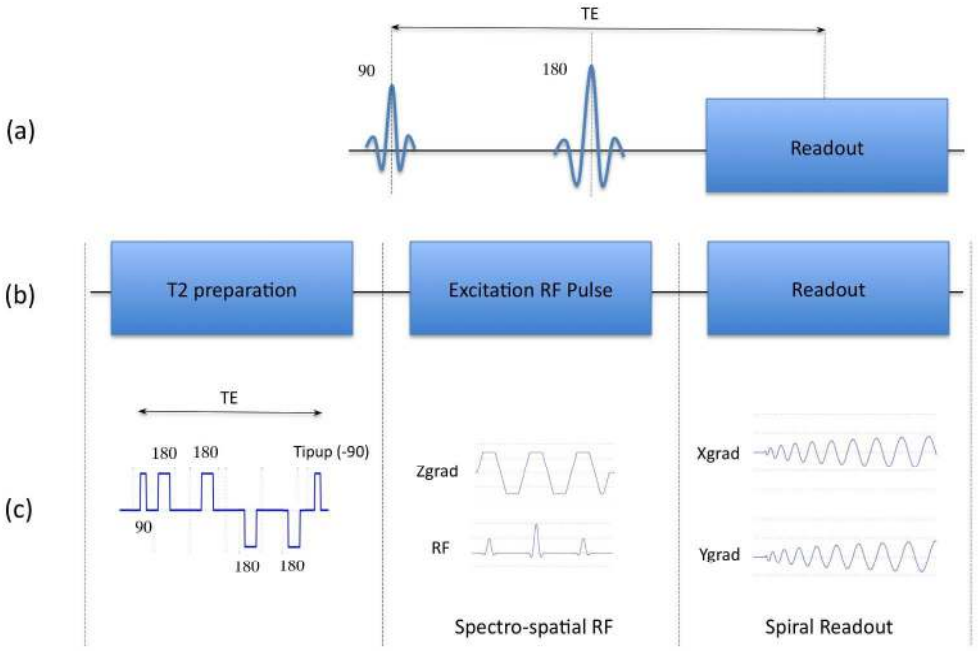

Figure 4: (a) Typical spin echo sequence for T2 measurement. (b) Magnetization preparation where T2-weighted contrast is prepared in advance of excitation and readout. (c) Example of a sequence using T2-preparation with a spectro-spatial RF excitation and spiral readout; TE is determined by the number of 180 refocussing pulses.
227x151mm (300 x 300 DPI)

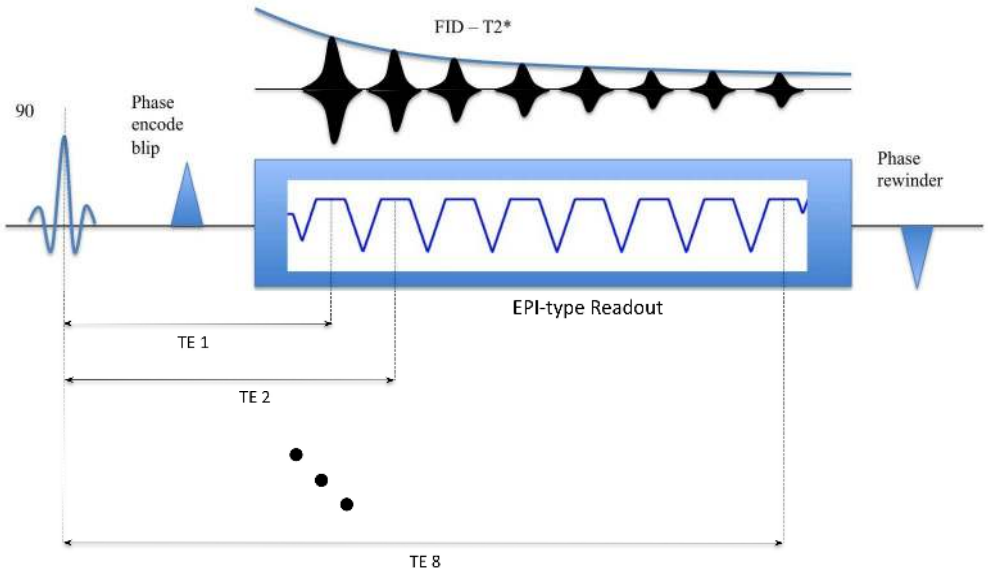

Figure 5: Multi-echo gradient echo sequence with echo-planar-imaging (EPI-type) readout for the measurement of T2*. Eight echos are typically acquired ranging from 2-15 ms with TR=20 ms. The free-induction-decay (FID) is shown with exponential time constant T2*.
229x137mm (300 x 300 DPI)

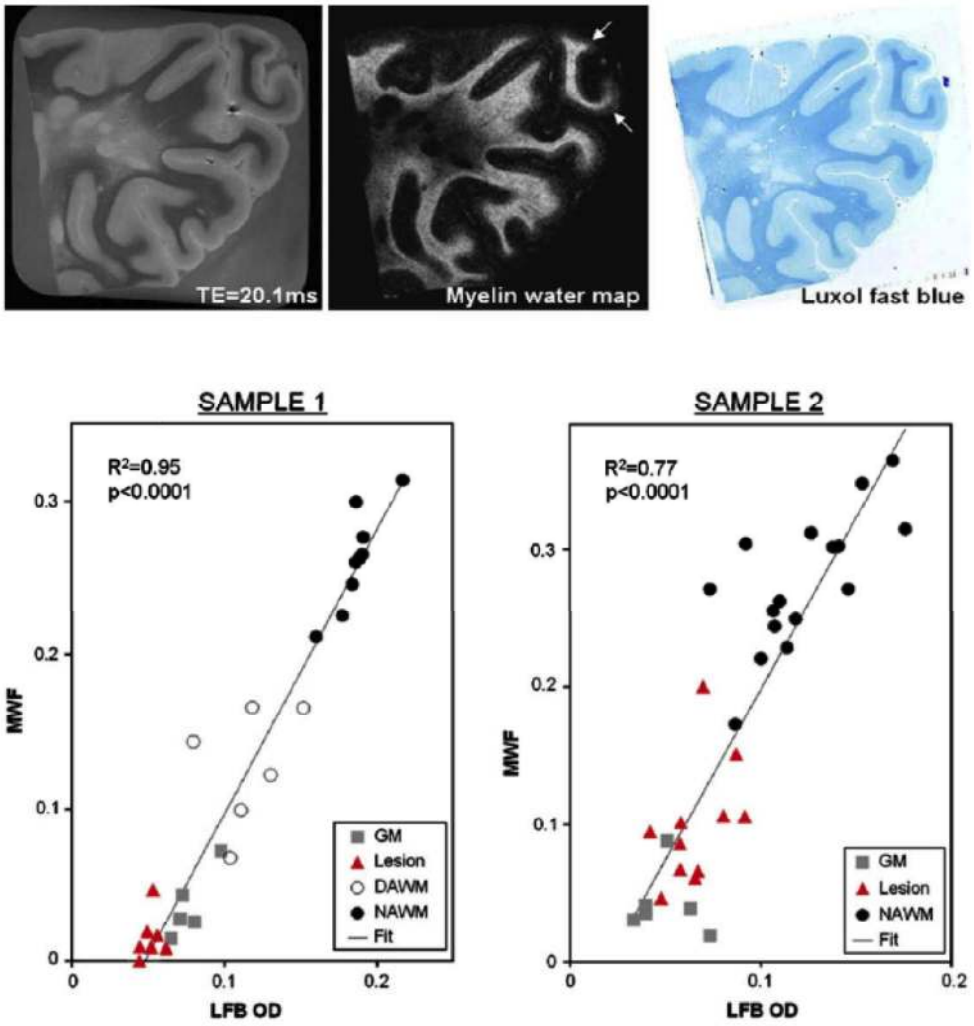

Figure 6: (Top) Example of a 7.0 T TE = 20.1 ms image and myelin water fraction (MWF) map and corresponding luxol fast blue histology image of the parieto-occipital region of a patient who has MS. A good qualitative correspondence is observed between the MWF map and histology stain for myelin. The normal prominent myelination of the deeper cortical layers (arrows) is also visible on the myelin water image. (Bottom) Examples of the quantitative correlation between myelin water fraction (MWF) and luxol fast blue optical density (LFB OD) for gray matter (GM), lesion, dirty-appearing white matter (DAWM), and normal appearing white matter (NAWM) for two MS samples (from MacKay et al. MR Relaxation in Multiple Sclerosis Nueroimag Clin N Am 19 (2009) 1-26; with permission).
158x163mm (300 x 300 DPI)

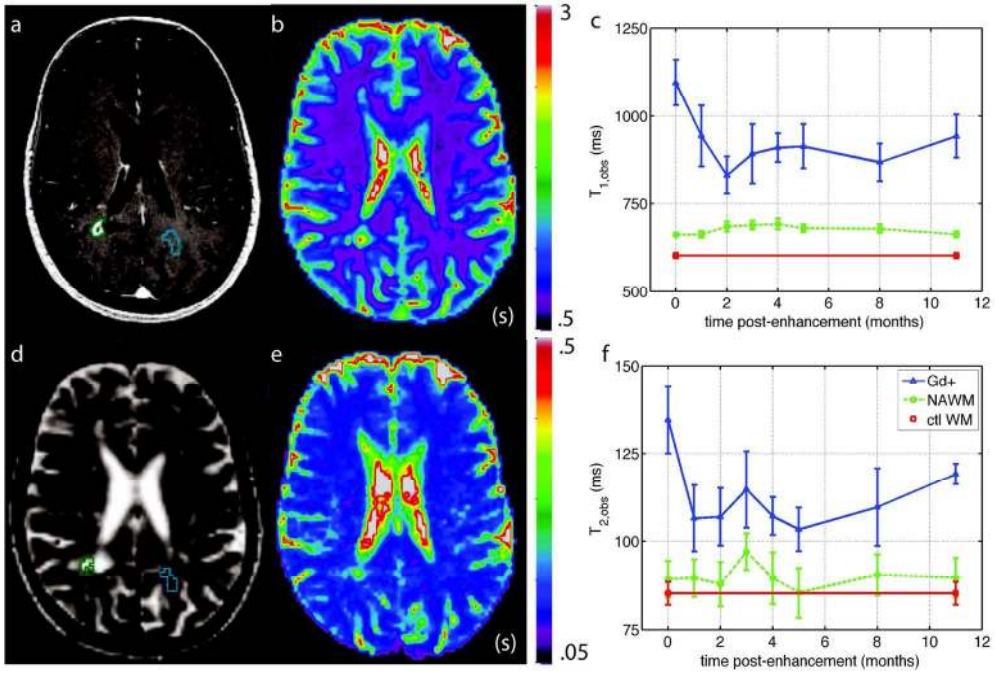

Figure 7. a) Initial post-Gd T1-weighted scan of a single patient with outlines of enhancing region (green) and contralateral NAWM (cyan) b) T1 map of the same subject (units are s) c) Plot of T1, averaged across five subjects at 8 time-points distributed over 12 months, starting at initial Gd enhancement. Error bars indicate the standard error of the mean across subjects d) T2-weighted image resampled to the lower resolution of the quantitative maps e) T2 map of the same subject (units are s) f) Plot of T2, averaged across five subjects at 8 time-points distributed over 12 months, starting at initial Gd enhancement. Error bars indicate the standard error of the mean across subjects (adapted from Levesque et al. Magn Reson Med, 2010, 63:633-640; with permission). Gd = Gadolinium.
146x98mm (300 x 300 DPI)

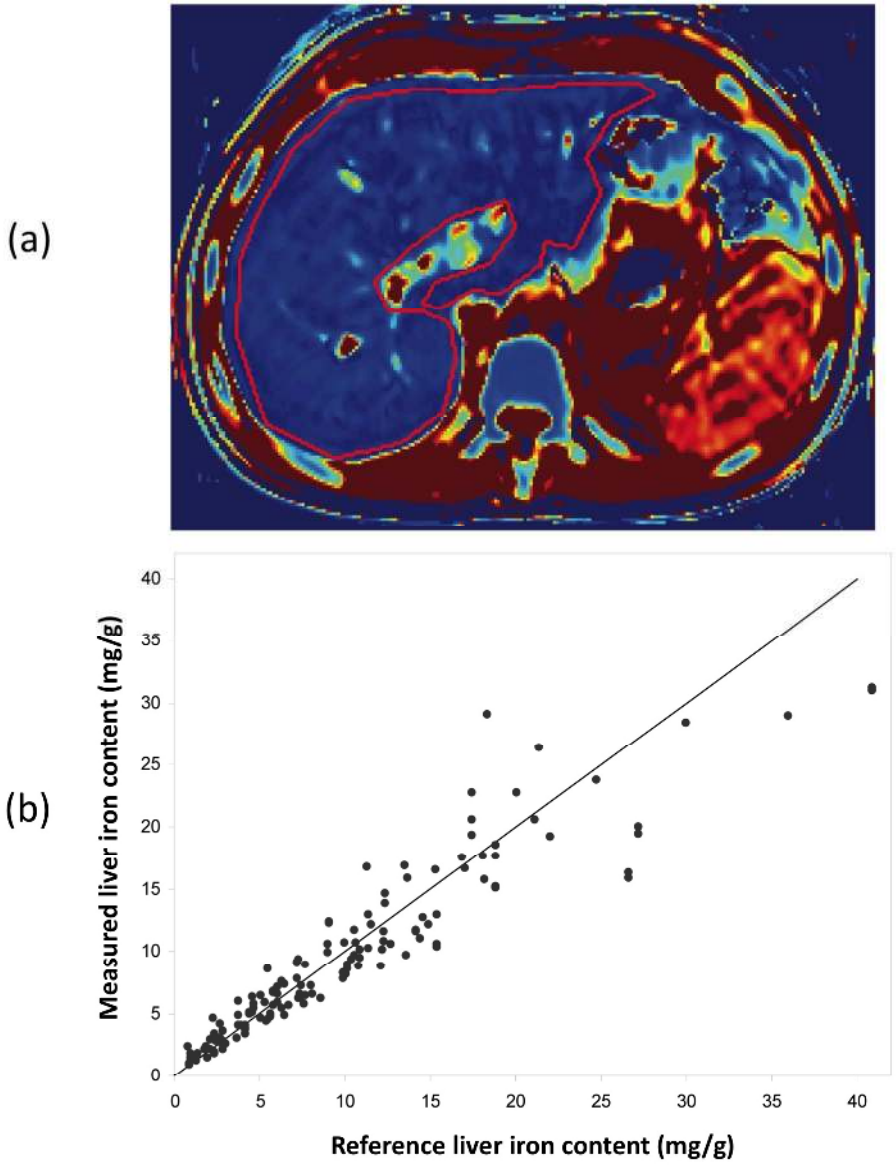

Figure 8: Absolute liver iron measurement in children. (a) Coronal image slice showing the T2* relaxation time distribution in the liver of a patient with iron overload. Red outline was manually drawn to contour the liver. (b) Measured absolute liver iron from T2* relaxation times compared against reference measurements in 151 pediatric patients (r = 0.94). Line of identity is shown.
143x182mm (300 x 300 DPI)

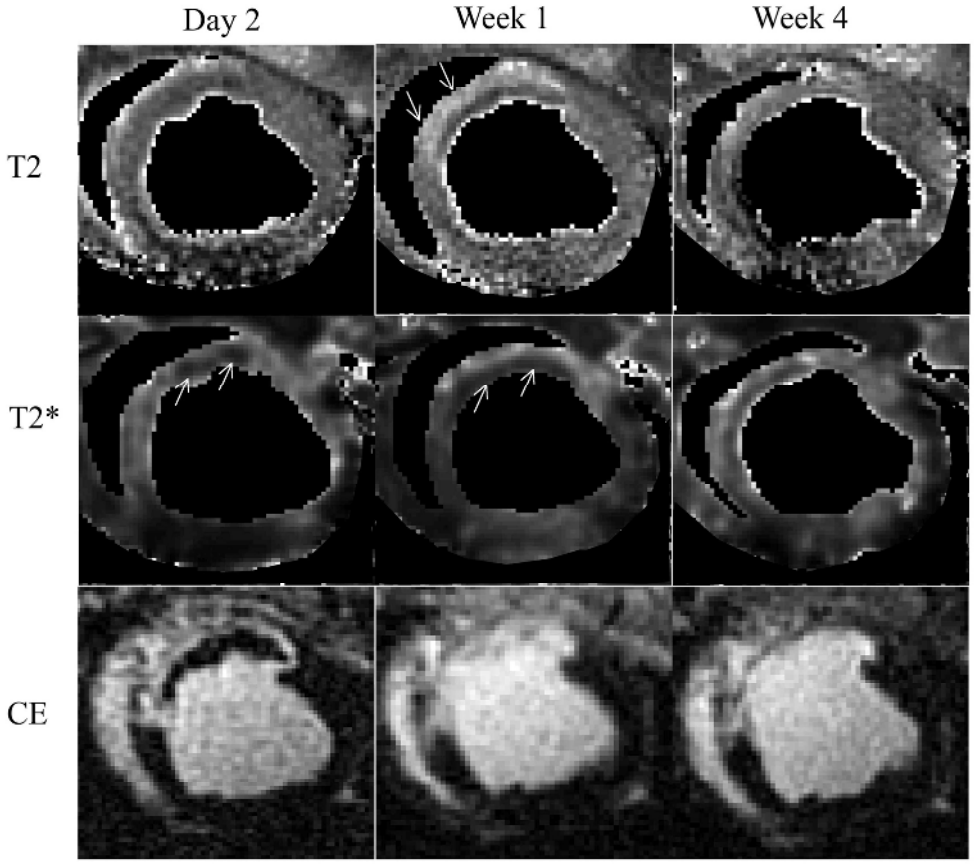

Figure 9: Longitudinal changes in edema, hemorrhage and MVO. T2 and T2* maps are shown along with early contrast enhanced (CE) images at various time points post-AMI in a porcine model of myocardial infarction. Day 2: T2 elevation usually associated with edema was not apparent in the infarct zone (39.2 ms vs. 39.1 ms control) but T2 was slightly elevated in the peripheral areas; Arrows indicate focal signal-void regions or T2* abnormalities (18.5 ms vs. 34.2 ms control) within the MVO as delineated by the CE image. Week 1: T2 was elevated (arrows) in most of the infarct (51.1 ms) with reduced sub-endocardial T2* (15.8 ms) indicative of diffuse hemorrhagic by-products (arrows). Week 4: T2 was still elevated (50 ms) while normalization of T2* (35 ms) coincided with resolution of MVO. (Reproduced from Ghugre et al., Magn Reson Med, 2011, 66(4): 1129-41; with permission).
155x138mm (300 x 300 DPI)

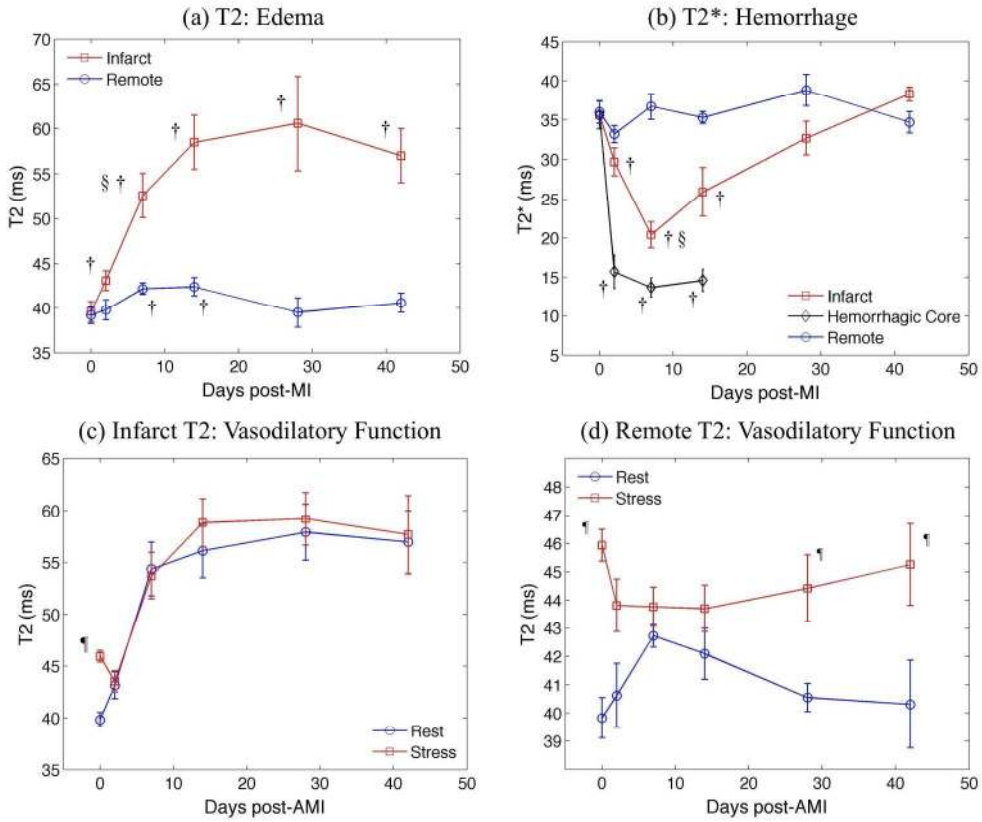

Figure 10: Quantitative fluctuations in relaxation parameters after AMI. Plots (a) and (b) demonstrate longitudinal fluctuations in T2 and T2* in the infarct zone compared to remote myocardium averaged over all animals; day 0 represents values from healthy controls and error bars represent standard error. Plots (c) and (d) show evolution of T2 in the rest and stress states (dipyridamole induced pharmacological vasodilation) in infarcted and remote myocardium, respectively; the difference between the two states is a reflection of vasodilaory function or myocardial perfusion reserve. † $p<0.05$, compared to control values; § $p<0.05$, compared to the previous time point; ¶ $p<0.05$ compared to rest values. (Modified from Ghugre et al., Magn Reson Med 2011, 66(4): 1129-41 and Ghugre et al., Magn Reson Med, 2011, 66(6):1739-1747; with permission).
200x168mm (300 x 300 DPI)